Nanosecond optical parametric oscillators and amplifiers based on periodically poled $KTiOPO_4$

Jonas Hellström

Doctoral thesis

Department of Physics
The Royal Institute of Technology
Stockholm, Sweden 2001

Nanosecond optical parametric oscillators and amplifiers based on periodically poled $KTiOPO_4$

Jonas Hellström
ISBN 91 – 7283 – 214 - 2

Doktorsavhandling vid Kungliga Tekniska Högskolan
TRITA-FYS 2001:5
ISSN 0280-316X
ISRN KTH/FYS- -01:5- -SE

Laser Physics and Quantum Optics group
Department of Physics
The Royal Institute of Technology
SCFAB
SE-106 91 Stockholm, Sweden.
Telephone: +46-8-5537 8000

Cover: Non-phasematched parasitic wavelengths generated by an optical parametric oscillator.

Printed by Universitetsservice US-AB, Tryck & Media
Stockholm, 2001.

Hellström, Jonas
Nanosecond optical parametric oscillators and amplifiers based on periodically poled $KTiOPO_4$.
Laser Physics and Quantum Optics, Department of Physics, The Royal Institute of Technology, SCFAB, SE-106 91 Stockholm, Sweden. TRITA-FYS 2001:5.

Abstract

Optical parametric oscillators (OPOs) and optical parametric amplifiers (OPAs) constitute a class of optical frequency converting devices that have many possible applications, e.g. in range finding, molecular spectroscopy and medicine. They can convert the frequency of the incident pump field with high efficiency, and generate two waves at new frequencies that will be continuously tuneable over a wide spectral range. Virtually any wavelengths within the transparency region of the nonlinear material can be generated if the material can be quasi-phasematched (QPM). In addition, QPM gives the possibility to utilise the largest nonlinear tensor element of the material and allows walk-off free interaction between the waves.

The aims of this thesis have been to investigate the possibility to use QPM $KTiOPO_4$ crystals as nonlinear material in nanosecond OPOs and OPAs operating at room-temperature, and to explore the advantages and shortcomings of these devices. The technique of electric field poling has been employed to implement the QPM structure in flux grown $KTiOPO_4$ (KTP).

The main conclusion is that periodically poled KTP (PPKTP) is a suitable material to use in nanosecond OPOs and OPAs. The material properties that foremost make KTP into an attractive nonlinear material are: The large value of the nonlinear coefficient d_{33}, the high resistance to optically induced breakdown, the low susceptibility to grey-track formation, the insensitivity to the photorefractive effect, the wide transparency and the low coercive field.

The thesis shows that it is possible to pole large volumes of KTP with a high quality of the QPM structure. Highly efficient nanosecond OPOs have been constructed during this project. Maximum conversion efficiencies have reached 45 % in the case of a singly resonant OPO (SRO) built around a 3 mm thick PPKTP crystal. Total pulse energies for both the signal (1.72 μm) and the idler (2.8 μm) of up to 18 mJ was reached and an average output power of 2 W was obtained for this sample. However, up to 24 W was produced in a doubly resonant OPO operating close to degeneracy. The efficiency reached 48 % for that case. Truly continuous and very wide spectral tuning has also been demonstrated, as well as a narrow bandwidth OPO operating on one single longitudinal mode.

Keywords: optical parametric oscillators, optical parametric amplifiers, quasi-phasematching, $KTiOPO_4$, nonlinear optics, frequency conversion, periodic electric field poling, ferroelectrics, high-order second harmonic generation, electro-optic effect.

Preface

The work this thesis is based on was to the largest extent performed at the Laser Physics and Quantum Optics group, department of Physics, at the Royal Institute of Technology, Stockholm, Sweden from April 1998 to December 2001.

Fruitful collaborations within the framework of this thesis have been performed with the following research groups: Prof. R. Wallenstein's group at Kaiserslautern University, Germany, Prof. B. Boulanger's group at the University of Grenoble, France, Dr. G. W. Baxter, P. Schlup and Dr. I. T. McKinnie, University of Otago, Dunedin, New Zealand, Dr. Y. Hirano's group at Mitsubishi Electric Corporation, Ofuna, Japan, Prof. A. Piskarskas' group at Vilnius University, Lithuania, Dr. V. Petrov's group at the Max-Born Institute in Berlin, Germany and Profs. M. H. Dunn's and M. Ebrahimzadeh's group at St:Andrews University, Scotland.

The project was possible through generous grants from Göran Gustafssons stiftelse (my salary), Tekniskaforskningsrådet (equipment and travel), Helge Ax:son Johnsons stiftelse (equipment), Kungliga Vetenskapsakademien (travel) and Knut och Alice Wallenbergs stiftelse (travel).

This thesis contains an introductory part to give a theoretical and technological background to the journal papers that are reprinted at the end. The text also gives a very brief historical overview of the field of optical parametric down-conversion in nonlinear crystals and discusses some possible applications of the devices.

List of publications

Paper I: J. Hellström, V. Pasiskevicius, F. Laurell, and H. Karlsson, "Efficient nanosecond optical parametric oscillators based on periodically poled KTP, emitting in the 1.8 – 2.5 μm spectral region", Opt. Lett., **24**, 1233-1235 (1999).

Paper II: J. Hellström, V. Pasiskevicius, H. Karlsson, and F. Laurell, "High-power optical parametric oscillation in large-aperture periodically poled $KTiOPO_4$", Opt. Lett., **25**, 174-176 (2000).

Paper III: J. Hellström, G. Karlsson, V. Pasiskevicius, and F. Laurell, "Optical parametric amplification in periodically poled $KTiOPO_4$, seeded by an Er-Yb:glass microchip laser", Opt. Lett., **26**, 352-354 (2001).

Paper IV: J. Hellström, R. Clemens, V. Pasiskevicius, H. Karlsson, and F. Laurell, "Real-time and *in situ* monitoring of ferroelectric domains during periodic electric field poling of $KTiOPO_4$", J. Appl. Phys., **90**, 1489-1495 (2001).

Paper V: G. W. Baxter, P. Schlup, I. T. McKinnie, J. Hellström, and F. Laurell, "Single mode near infrared optical parametric oscillator–amplifier based on periodically poled $KTiOPO_4$", Accepted for publication in Appl. Opt., Dec, (2001).

Paper VI: J.-P. Fève, O. Pacaud, B. Boulanger, B. Ménaert, J. Hellström, V. Pasiskevicius, and F. Laurell, "Widely and continuously tuneable optical parametric oscillator using a cylindrical periodically poled $KTiOPO_4$ crystal", Accepted for publication in Opt. Lett., Dec (2001).

Paper VII: M. Peltz, U. Bäder, A. Borsutzky, R. Wallenstein, J. Hellström, H. Karlsson, V. Pasiskevicius, and F. Laurell, "Optical parametric oscillators for high pulse energy and high average power operation based on large aperture periodically poled KTP and RTA." Accepted for publication in Appl. Phys. B.

Paper VIII: F. Rotermund, V. Petrov, F. Noack, V. Pasiskevicius, J. Hellström, and F. Laurell, "Efficient femtosecond travelling-wave optical parametric amplification in periodically poled $KTiOPO_4$", Opt. Lett. **24**, 1874-1876 (1999).

Paper IX: V. Smilgevičius, A. Stabinis, A. Piskarskas, V. Pasiskevicius, J. Hellström, S. Wang, and F. Laurell, "Noncollinear optical parametric oscillator with periodically poled KTP", Opt. Comm. **173**, 365-369 (2000).

Other publications by the author related to the subject, but not included in this thesis.

Paper AI: S. Wang, V. Pasiskevicius, J. Hellström, F. Laurell, and H. Karlsson, "First-order type II quasi-phase-matched UV generation in periodically poled KTP", Opt. Lett., **24**, 978 (1999).

Paper AII: V. Pasiskevicius, H. Karlsson, J. Hellström, F. Laurell, and I. Freitag, "Low-threshold mid-infrared optical parametric oscillation in periodically poled $KTiOPO_4$", Proc. SPIE, **Vol. 3928**, 2 (2000).

Acknowledgements

First and foremost I would like to acknowledge my supervisor Prof. Fredrik Laurell for his never-ending support, guidance and encouragement throughout these years. He has always taken his time to listen to my big and small problems ever since he first accepted me as a Master Thesis student. Furthermore, I would like to thank him for giving me the opportunity to work in his group and from time to time sending me abroad to collaborate with his many colleagues and friends around the world.

I would also like to express my sincere gratitude to Dr. Valdas Pasiskevicius for sharing his vast knowledge in physics, especially nonlinear optics, with me. For innumerable discussions and for always having his office-door open.

I'm very grateful to Dr. Håkan Karlsson, for teaching me electric field poling, and for the poled crystals he provided during this thesis. I have very much appreciated the scientific and the non-scientific discussions in and outside the lab. It has been a great time in Stockholm, Paris, Cargese, San Fransisco and Baltimore.

I would like to thank all the present and former members of Fredrik's group, for all the fun at and after work! Thank you:
Rosalie Clemens and Gunnar Karlsson, for our successful collaborations, Stefan Spiekermann for philosophic discussions about all and everything (and his Kartoffelsalat), Carlota Canalias, Stefan Holmgren and Shunhua Wang (my room-mates) for pleasant office chit-chats, Assoc. Prof. Jens A. Tellefsen Jr, for arranging pool-parties and linguistic advice, Göran Hansson for sharing and discussing problems related to "*how to write a PhD-thesis*", David Koch for polishing crystals, Jonas E. Hellström (Junior) for having such a nice name and Lars-Gunnar Andersson, Anna Frageman, Sandra Johansson, and Mikael Tiihonen for being the most recent contribution of nice and fun people to the group.

Many thanks to our secretary Agneta Falk for keeping track of our bills and us. Many thanks also to our invaluable technician Rune Persson for all practical problems you solved. In addition, I would like to acknowledge colleagues and friends at the former section of Physics II - (Optics) for giving interesting courses, answering questions and pleasant coffee breaks. I'm also thankful towards the colleagues at ACREO AB for lending me valuable equipment, special thanks to Leif Kjellberg for all the help with the electrical circuits. Thanks a lot, Jenni Nordborg at Cobolt AB, for discussing material related issues of $KTiOPO_4$ and isomorphic compounds with me.

Furthermore, I want to communicate my appreciation to all the research groups that I have collaborated with during this thesis. The projects have been very fruitful and the visits to your laboratories and countries have been most enjoyable and I would like to once again thank you all.

A special thanks to Mark Peltz for his and his family's hospitality and all the fun in Germany, hope to see you all in Sweden soon.

I want to say that I'm very honoured and thankful towards Göran Gustafssons stiftelse for their decision to support me during these four years by providing my salary.

Dr. Weizhi Wang and Prof. Martin M. Fejer are acknowledged for a very interesting and enjoyable stay at Stanford University during my Master Thesis project. It is partly your “fault” that I decided to apply for a PhD-position and I would like to thank you for that once again.

Finally, I would like to express my appreciation to my family and friends. Thanks for the distraction from work and for your support!

Table of contents

1 Introduction

1.1 Background

In December 1958 A. C. Schawlow and C. H. Townes published a paper that would have a tremendous impact on the research field of optics. In that article they proposed, for the first time, that the maser principle should be possible to extend to the optical frequency part of the electromagnetic spectrum. In other words the laser was invented[1]. Maiman demonstrated the first laser only one and a half years later[2] and ever since the laser has grown in importance to both science and society alike. Today, lasers are part of everyday life. They sit in our CD-players and computers, we use them when we telephone over optical networks or when we surf the Internet, and they measure distances with acute accuracy and they can be used to detect extremely small amounts of environmental pollutants. These are but a few examples of possible applications. Perhaps the principal advantage with the laser is that it can convert spectrally incoherent energy, e.g. from a flash-lamp, to high brightness beams of highly coherent energy.

Unfortunately, the output of the laser can not have an arbitrary wavelength, although that would have been desirable, since the wavelength is governed by the energy levels of the atoms, ions or molecules that constitute the gain medium. Using the laser as a pump source in a frequency conversion process can circumvent this problem and provide output radiation at, in principle, any frequency in the entire spectral region from ultraviolet to far-infrared.

Optical parametric oscillators, amplifiers and generators constitute a class of frequency converting devices that is particularly interesting, since they can split the pump photon into two parts with potentially very high efficiency, and simultaneously the two generated waves will be continuously tuneable over a wide spectral range. Virtually any wavelength within the transparency region of the medium can be generated, if in addition the nonlinear material can be quasi-phasematched.

The two fundamental physical relationships that have to be met for an optical parametric device to function are conservation of photon energy and momentum. Quasi-phasematching means that the nonlinear material is manipulated in an ordered fashion in such a way that an extra artificial momentum vector is added to the momentum conservation equation. This can, for example, be done by periodically inverting the spontaneous polarisation of a ferroelectric material through electric field poling. The fact that the momentum equation can be tailored adds an enormous amount of flexibility and possibilities to the field of nonlinear optics. The many advantages that quasi-phasematching provides have, during the last decade, led to an ever increasing interest in quasi-phasematched nonlinear optical devices both from academia and industry.

Applications for these devices are identical to the applications of the laser with the addition that the spectral output can be easily tailored and new wavelength regions can be reached. However, this does not imply that parametric devices are always better to use than lasers. The choice of source for coherent light generation depends on the specific requirements of the particular application. Possible applications where

parametric devices might be advantageous are, for example, in molecular spectroscopy where one optical parametric oscillator (OPO) with a narrow bandwidth can be tuned over many absorption lines to detect a spectrum of molecules. OPOs can provide radiation in the mid-infrared spectral range for dental surgery and for tissue ablation. They can convert intense pulses of pump radiation at 1.064 μm to the "eye-safe" region at 1.55 μm, in order to use the pulses in range finding applications e.g. velocity measurements of cars can be made at large distances without the risk of damaging the eyes of the driver etc. The fact that two wavelengths are generated simultaneously has also led researchers to propose that an OPO pumped by ultraviolet light could be used in laser display applications or laser TVs. The OPO would then provide both red and blue light at the same time and only green light would be required from another source to make the colour image.

1.2 The aim of this thesis

The aims of this thesis project have been to investigate the possibilities to use quasi-phasematched $KTiOPO_4$ crystals as nonlinear material in nanosecond optical parametric oscillators (OPOs) and optical parametric amplifiers (OPAs), and to explore the advantages and shortcomings of these devices compared to existing devices which are based on other materials. The targeted wavelength regions for the output wavelengths have been the near and mid-infrared spectral ranges. The questions that were asked at the beginning of the project and which had to be addressed were:

Is it possible to periodically electric field pole $KTiOPO_4$ crystals with a sufficiently high quality over large volumes to make the quasi-phasematched material suitable as nonlinear material in nanosecond OPOs and OPAs?

Are the optical, dielectric, ferroelectric and mechanical properties of periodically poled $KTiOPO_4$ suitable for making the parametric frequency conversion process efficient?

What kind of parasitic processes that are detrimental to the desired frequency conversion can occur and how severe will they be?

In particular during this project, I wanted to prove that it is possible to construct nanosecond OPOs and OPAs in periodically poled $KTiOPO_4$ that are tuneable over a wide range of the infrared part of the spectrum, with possible applications in molecular spectroscopy in mind. I also wanted to show that the fabricated devices could be efficient and able to handle both high average powers and high pulse energies. To be able to construct an OPO with a narrow bandwidth for spectroscopic purposes was also desired.

Refining the monitoring technique used during the electric field poling was an additional objective in this project.

1.3 Method

The method used in this thesis to answer the questions and address the statements above has been more or less purely experimental. Existing theory has been used to verify that the experiments gave credible results and to help explain the observed phenomena.

1.4 Evolution of the project

After initial studies of the literature, a birefringent phasematched OPO in $KTiOPO_4$ was implemented in order to gather knowledge regarding OPO performance in general. This was to my knowledge the first OPO ever in our laboratory. After that, 1 mm thick periodically poled samples of $KTiOPO_4$ (PPKTP) were fabricated to be used in OPOs. The OPO cavities were designed from further studies of the literature and with the help of computer simulations. The demonstrated nanosecond PPKTP OPOs were the first of their kind reported and they showed promising efficiencies and output pulse energies [I]. The next step was to scale the output energies. For this purpose a 3 mm thick PPKTP OPO was constructed and a large pump beam area was used to produce output pulses in the 10 mJ range, [II]. The device efficiency was high and led us to try optical parametric amplification in PPKTP. The laser radiation from an Er-Yb:glass laser was amplified and although the available PPKTP crystal length with the correct period was only 12 mm at that time, a 66 dB amplification of the signal radiation at 1.54 μm was achieved [III]. In order to construct an OPO with a very narrow output bandwidth it is advantageous to have an injection seeded pump laser, which provides a narrow pump bandwidth. Since such a laser was not available in our laboratory, collaboration with a research group from New Zealand was initiated. The result of this joint project is the OPO presented in paper [V]. As mentioned, we also wanted to demonstrate a wide tuning range for the PPKTP OPOs. This led to collaboration with a French research group, where a PPKTP sample was polished to a cylindrical shape. The shape of the crystal enabled the OPO to be widely and continuously tuneable [VI]. A third collaboration was set up with a German group, with whom we investigated the homogeneity of the poled volume of the 3 mm thick PPKTP sample in detail. High average power experiments, as well as further experiments on high pulse energy generation were also performed [VII]. Furthermore, the tuning characteristics of a non-collinearly phasematched PPKTP OPO operating close to degeneracy were investigated experimentally and theoretically in paper [IX] in collaboration with a research group from Lithuania. Finally, a brief investigation of the benefits and drawbacks in using PPKTP as nonlinear material in a femtosecond OPO was reported [VIII].

A novel monitoring technique to view the inversion of the ferroelectric domains during electric field poling has been developed within the framework of this thesis. To be well informed about how the domain inversion proceeds during periodic poling is very important in order to fabricate quasi-phasematched structures with high quality [IV].

1.5 Outline of the thesis

This thesis report can be outlined as follows: Chapter 2 presents an introduction to the field of nonlinear optics and in particular second order nonlinear frequency mixing processes. In chapter 3 the basic theory of quasi-phasematching is presented and different techniques to implement quasi-phasematching are discussed, as well as advantages and disadvantages of quasi-phasematching compared to birefringent phasematching. Chapter 4 deals with the material properties of $KTiOPO_4$ and compounds that are isomorphic with $KTiOPO_4$. Optical damage mechanisms that may occur in $KTiOPO_4$ are also discussed. Chapter 5 contains the description of how the electric field poled samples in this thesis were fabricated. The photographic method developed to monitor the periodic poling *in-situ* and in real time is also presented here in detail. The chapter includes an additional short paragraph on how the quality of the PPKTP samples was evaluated immediately after poling. In the introduction to chapter 6 a short historical background to the field of nonlinear optics and optical parametric devices is given. After this, a comparison of PPKTP and other nonlinear materials that could be used in OPOs and OPAs is presented. In the remaining part of chapter 6 the basic theory for OPAs and OPOs is given and the most important experimental results for the OPAs and OPOs in this thesis are presented. Comparisons are made with OPOs built around periodically poled $LiNbO_3$, since $LiNbO_3$ is the most extensively used material both in quasi-phasematched and birefringently phasematched OPOs. At the end of the chapter the parasitic processes that were observed in the experiments are discussed. Chapter 7 contains a summary of the original research work. In chapter 8, I describe which specific parts of the work in each paper that I have performed. Finally, the conclusions are presented in chapter 9.

2 Nonlinear optics

2.1 The nonlinear polarisation

Optical phenomena that we observe in our every day life, e.g. refraction in a glass prism or the colours from the interference pattern of an oil film on water can to a very high degree of accuracy be describe by linear equations. Dielectric media like glass or water may be thought of as an assembly of positive ion cores, where each core is surrounded by a negatively charged electron cloud. In linear optics, the electromagnetic wave induces a polarisation in the dielectric material, i.e. a separation of charges, which is directly proportional to the electric field and hence oscillates with the same frequency as the applied field. The linearity also implies that the electromagnetic waves passing through the material do not interact with each other or themselves to create waves at new frequencies and that the observed phenomena is not dependant of the light intensity.

However, if the electric fields become sufficiently strong it will disturb the electron cloud to the degree when the restoring forces between the heavy ion cores and electrons are not linear to the electric field anymore. It is then not enough to describe the induced polarisation with a linear term, instead a full series expansion of the polarisation in terms of successively higher orders of the electric field is needed.

$$\boldsymbol{P} = \varepsilon_0 \chi^{(1)} \boldsymbol{E} + \varepsilon_0 \left(\chi^{(2)} \boldsymbol{E}^2 + \chi^{(3)} \boldsymbol{E}^3 + \ldots \right) = \boldsymbol{P}^{\mathrm{L}} + \boldsymbol{P}^{\mathrm{NL}} \qquad 2.1$$

Here $\mathbf{P}^{\mathrm{L}}$ denotes the linear part of the polarisation, $\mathbf{P}^{\mathrm{NL}}$ the nonlinear part, ε_0 is the permittivity of vacuum, $\mathbf{E}$ is the electric field component of the electromagnetic wave and $\chi^{(m)}$ represents the susceptibility tensor of m:th order with the rank (m+1). To observe consecutively higher orders of nonlinear phenomenon the electric field must become stronger and stronger, since the magnitude of the susceptibility tensor elements falls off rapidly with increasing order.

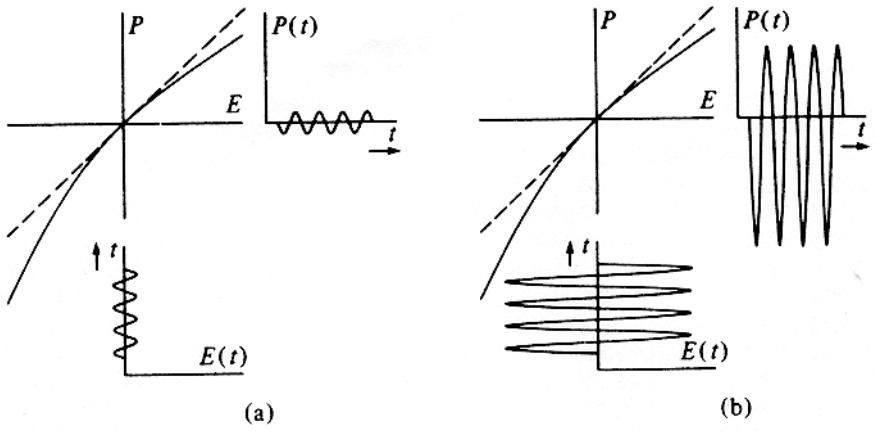

Fig. 2.1 The nonlinear dependence of the polarisation versus the applied electric field. (a) small input fields result in a linear response. (b) strong input fields causes a distorted waveform of the polarisation, which contains harmonic frequencies[3].

The quadratic polarisation $\mathbf{P}^{(2)} = \varepsilon_0\chi^{(2)}\mathbf{E}_1\mathbf{E}_2$ is responsible for many interesting effects. In the case when both electric fields oscillate with optical frequencies, different types of frequency conversion processes occur, figure 2.2, while if one field is static the refractive index of the media is affected through the linear electro-optic effect, (the Pockel's effect). For all frequency conversion processes the energy of the photons that take part in the mixing has to be conserved. The frequency conversion processes may be divided into two groups. In the first, two electromagnetic waves with different frequencies are impinging on the media. Sum-frequency generation (SFG) take place when the photon energies from the different fields are added and a photon with higher energy is created. Difference-frequency generation (DFG) occurs when the photons with lower energy are subtracted from the photons with higher energy. At the same time the light waves can also interact with themselves and create a polarisation, which contains both a static component (dc-rectification) and one at the double original frequency, second harmonic generation (SHG). In the second group there is only one field, the pump field, incident to the material. A pump photon is split up into two photons with lower energy, this is called optical parametric generation (OPG). The generated photons are denoted signal and idler photons, where the former has higher frequency than the latter. If a cavity is used to enhance the efficiency by resonating one or both of the generated fields, the device is named an optical parametric oscillator (OPO). Finally, optical parametric amplification (OPA) is essentially an OPG process where either the signal or the idler fields are seeded on the incoming side. OPA may also be considered to be a sort of difference frequency process, but in the case of OPA the amplification of the seed field is studied, while on the other hand for DFG the idler field gets most attention.

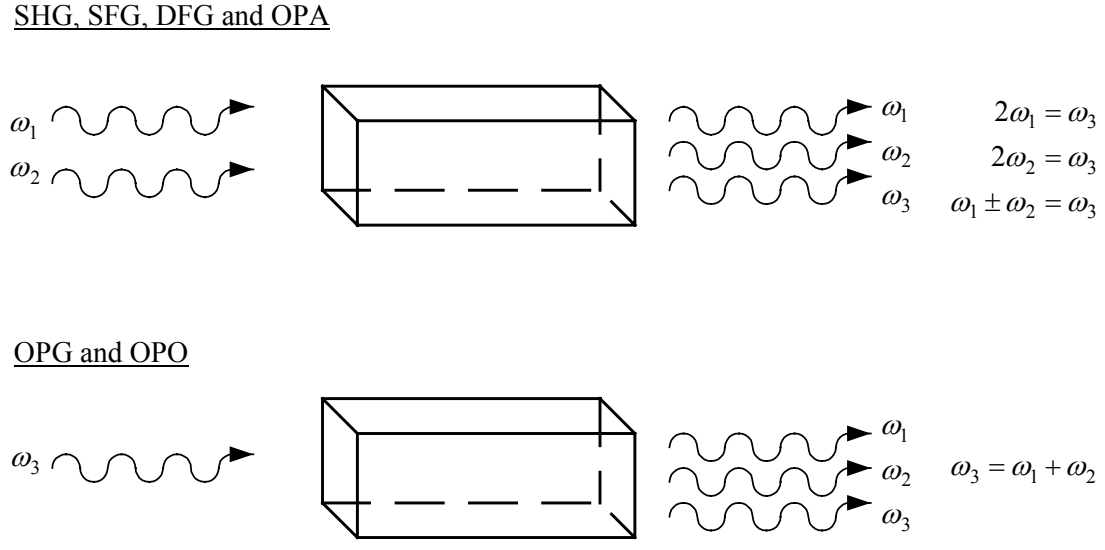

Fig. 2.2 Frequency conversion processes arising from $\chi^{(2)}$.

The cubic polarisation $\mathbf{P}^{(3)} = \varepsilon_0\chi^{(3)}\mathbf{E}_1\mathbf{E}_2\mathbf{E}_3$ causes the quadratic electro-optic effect (the dc Kerr effect), dc induced SHG, four wave mixing processes, the optical Kerr effect, two photon absorption, Raman and Brillouin scattering.

This thesis focuses on parametric down conversion in particular OPOs and OPAs.

Even orders of the polarisation can only exist in material that lacks a centre of inversion. Among the 32 different crystal classes in nature 21 are acentric[3]. The second order susceptibility is in the literature most often replaced by the second order nonlinear tensor, the d-tensor[3-6]. The relation between the tensors is:

$$\chi^{(2)}_{ijk}(-\omega_3;\omega_1,\omega_2) = 2d_{ijk}(-\omega_3;\omega_1,\omega_2) \tag{2.2}$$

The d-tensor consists of 27 elements, but in the case of frequency doubling the intrinsic permutation symmetry of the tensor allows it to be contracted to a matrix of 3 by 6 independent elements. This contraction of the original tensor can be done for any second-order mixing process, if Kleinmann symmetry holds[7], i.e. all interacting frequencies are far from resonance. Furthermore, if the symmetry of the specific crystal class is taken into account the number of independent elements can be reduced further. The connection between the polarisation and the electric fields via the contracted tensor is written in matrix form as follows:

$$\begin{bmatrix} \left(P^{(2)}_{\omega_3}\right)_x \\ \left(P^{(2)}_{\omega_3}\right)_y \\ \left(P^{(2)}_{\omega_3}\right)_z \end{bmatrix} = 2\varepsilon_0 K \begin{bmatrix} d_{11} & d_{12} & d_{13} & d_{14} & d_{15} & d_{16} \\ d_{21} & d_{22} & d_{23} & d_{24} & d_{25} & d_{26} \\ d_{31} & d_{32} & d_{33} & d_{34} & d_{35} & d_{36} \end{bmatrix} \begin{bmatrix} \left(E_{\omega_1}\right)_x\left(E_{\omega_2}\right)_x \\ \left(E_{\omega_1}\right)_y\left(E_{\omega_2}\right)_y \\ \left(E_{\omega_1}\right)_z\left(E_{\omega_2}\right)_z \\ \left(E_{\omega_1}\right)_y\left(E_{\omega_2}\right)_z + \left(E_{\omega_2}\right)_y\left(E_{\omega_1}\right)_z \\ \left(E_{\omega_1}\right)_x\left(E_{\omega_2}\right)_z + \left(E_{\omega_2}\right)_x\left(E_{\omega_1}\right)_z \\ \left(E_{\omega_1}\right)_x\left(E_{\omega_2}\right)_y + \left(E_{\omega_2}\right)_x\left(E_{\omega_1}\right)_y \end{bmatrix} \tag{2.3}$$

$K(-\omega_3;\omega_1,\omega_2)$ is the degeneracy factor, which takes the value ½ for SHG and optical rectification and 1 for the other conversion processes. ω is the carrier frequency of the electromagnetic wave.

2.2 The coupled wave equations

Maxwell's equations and the constitutive relations[6] are the starting points to formally describe how the interaction between the different electromagnetic waves in the frequency conversion process evolves. Eliminating the magnetic field from Maxwell's equations leads to the following equation, which tells us how the generated electric field in the medium depends on the driving polarisation:

$$\nabla^2 \boldsymbol{E} = \mu_0\sigma\frac{\partial \boldsymbol{E}}{\partial t} + \mu_0\varepsilon_0\frac{\partial^2 \boldsymbol{E}}{\partial t^2} + \mu_0\frac{\partial^2 \boldsymbol{P}}{\partial t^2} \tag{2.4}$$

μ_0 is the permeability of vacuum and σ represents the losses of the material. In the following it is assumed that the electromagnetic waves are monochromatic. It is common to substitute the instantaneous fields in equation 2.4 with their Fourier components and to further simplify the problem by restricting the waves to only propagate along one axis e.g. the x-axis.

$$\begin{aligned} \boldsymbol{E}(x,t) &= \tfrac{1}{2}\left[\boldsymbol{E}(x,\omega)\exp i(kx-\omega t)\right] + c.c. \\ \boldsymbol{P}(x,t) &= \tfrac{1}{2}\left[\boldsymbol{P}(x,\omega)\exp i(kx-\omega t)\right] + c.c. \end{aligned} \tag{2.5}$$

The envelope functions are here assumed to be infinite plane waves. If it is reasonable to assume that the envelope is changing slowly both in amplitude and phase with distance, it is possible to apply the "slowly varying envelope approximation", SVEA.

$$\left|\frac{\partial^2 \boldsymbol{E}(\omega)}{\partial x^2}\right| << \left|k\frac{\partial \boldsymbol{E}(\omega)}{\partial x}\right|, \left|\frac{\partial \boldsymbol{E}(\omega)}{\partial t}\right| << \left|\omega \boldsymbol{E}(\omega)\right|$$
$$\left|\frac{\partial^2 \boldsymbol{P}(\omega)}{\partial t^2}\right| << \left|\omega\frac{\partial \boldsymbol{P}(\omega)}{\partial t}\right| << \left|\omega^2 \boldsymbol{P}(\omega)\right| \qquad 2.6$$

Invoking SVEA is the same thing as neglecting the component of the field generated by $\mathbf{P}^{NL}$, which is travelling backwards from the point of generation[8]. In equation 2.6, the wavenumber is denoted $k = n\omega/c$ where n is the refractive index and c is the speed of light in vacuum. The approximation reduces the second-order differential equation 2.4 to an ordinary differential equation, which is written for the forward travelling wave as:

$$\frac{\partial \boldsymbol{E}(\omega)}{\partial x} = -\alpha \boldsymbol{E}(\omega) + \frac{i\mu_0 c\omega}{2n}\boldsymbol{P}^{NL}(\omega) \qquad 2.7$$

$\alpha = \mu_0\sigma c/2$ is the loss coefficient of the electric field. For the $\chi^{(2)}$ mixing the three waves couple to each other through three polarisations, since all fields mix with all other. This yields three coupled wave equations, here in their scalar form:

$$\frac{\partial E_1}{\partial x} = -\alpha_1 E_1 + \frac{i\omega_1^2}{k_1 c^2} K d_{eff} E_3 E_2^* \exp(i\Delta k x)$$
$$\frac{\partial E_2}{\partial x} = -\alpha_2 E_2 + \frac{i\omega_2^2}{k_2 c^2} K d_{eff} E_3 E_1^* \exp(i\Delta k x) \qquad 2.8$$
$$\frac{\partial E_3}{\partial x} = -\alpha_3 E_3 + \frac{i\omega_3^2}{k_3 c^2} K d_{eff} E_1 E_2 \exp(-i\Delta k x)$$

The phase-mismatch equals $\Delta k = k_3 - k_2 - k_1$ and the frequency relation is $\omega_3 = \omega_1 + \omega_2$. The effective nonlinear coefficient, d_{eff}, for the studied process links the different polarisation directions of the interacting fields together and is obtained from the matrix in equation 2.3 modified with a coefficient for the relevant phasematching condition.

2.3 Second harmonic generation

Frequency doubling is probably the simplest frequency conversion process to study in order to gain some further insight into the interplay of the electric fields. Assume now that the incident fields to the media are degenerate with frequency $\omega_1 = \omega_2 = \omega$, i.e. indistinguishable and that a field at $\omega_3 = 2\omega$ is generated. If the material is lossless the equation system 2.8 is reduced to,

$$\frac{\partial E_\omega}{\partial x} = \frac{i\omega}{n_\omega c} d_{eff} E_{2\omega} E_\omega^* \exp(i\Delta k x)$$
$$\frac{\partial E_{2\omega}}{\partial x} = \frac{i\omega}{n_{2\omega} c} d_{eff} E_\omega E_\omega \exp(-i\Delta k x) \qquad 2.10$$

where the degeneracy factor has been replaced by its proper value and $\Delta k = k_{2\omega} - 2k_\omega$. In the next step it is assumed that the pump beam is not depleted when it propagates through the material. The lower equation in 2.10 can then be directly integrated over the crystal distance L. Keeping in mind that the intensity of each wave is $I_j = \frac{1}{2}\varepsilon_0 c n_j |E|^2$ gives:

$$I_{2\omega} = \frac{2\omega^2 d_{eff}^2 L^2 I_\omega^2}{n_{2\omega} n_\omega^2 \varepsilon_0 c^3} sinc^2\left(\frac{\Delta k L}{2}\right) \qquad 2.11$$

The function sinc(ξ) = sin (ξ)/ξ. The equation above illustrates the growth of the harmonic field versus distance in the lose-focussing limit, i.e. where the assumption of plane waves is valid. As seen the generated field increases with the length and the nonlinear coefficient squared. Boyd and Kleinman have also treated other focussing conditions in detail assuming a Gaussian spatial profile of the beam[9]. For a derivation of the SHG field when pump depletion is taken into account see refs. [6] or [10]. In experiments it is often easiest to measure the power P of the beam $I_j = P_j/A_j$, where A_j is the beam cross section. For a laser beam with a Gaussian spatial profile the effective area is $A = \pi(w_0)^2/2$ [6], w_0 is the beam radius where the intensity has reduced to $1/e^2$ (~13.5 %) of the peak value.

2.4 Phasematching

In principle all the mixing processes in figure 2.2 will occur simultaneously when an acentric crystal is pumped by intense beams, but most often only one process will grow strong over distance. The prevailing type will be the one for which the momentum of the photons that take part in the frequency conversion is conserved. For frequency doubling it can be seen from equation 2.11 that the intensity at 2ω will oscillate back and forth when the wave is propagation through the material, if the phase-mismatch is not zero,

$$\Delta k = k_{2\omega} - 2k_\omega = \frac{2\omega(n_{2\omega} - n_\omega)}{c} \neq 0 \qquad 2.12$$

The physics behind equation 2.12 is that the fronts of constant polarisation for $P_{2\omega}$ moves with the phase velocity of the pump field i.e., c/n_ω, while on the other hand the generated wave, $E_{2\omega}$, has the phase velocity $c/n_{2\omega}$. The driving polarisation and the generated field will thus drift out of phase relative each other. After the distance L_c, the coherence length, the fields have accumulated a phase shift of π between each other and the energy will start to flow in the opposite direction instead, from the harmonic field back to the field at the fundamental frequency.

$$L_c = \left| \frac{\pi}{\Delta k} \right| \qquad 2.13$$

In general $n_{2\omega} \neq n_{\omega}$, due to the dispersion of the material, nevertheless phasematching can be achieved by utilising different techniques. Probably the most common technique so far has been birefringent phasematching, BPM. There are two types of BPM, referring to figure 2.2: For type I both fields at frequencies ω_1 and ω_2 have the same polarisation, and the third field is polarised orthogonal compared to the two first. For type II the fields at ω_1 and ω_2 are orthogonally polarised.

In an uniaxial birefringent medium the refractive indices along the principle axes are $n_x = n_y = n_o$ and $n_z = n_e$, where n_o is the ordinary and n_e the extraordinary refractive index. The extraordinary wave has its polarisation in the plane containing the optical axis (z-axis) and the wavevector, **k**, of the wave and it will experience a refractive index $n_e(\theta)$ that changes depending on the propagation direction. The angle θ is the angle between the wavevector and the optical axis.

$$n_e(\theta) = \left[\frac{\sin^2\theta}{n_e^2} + \frac{\cos^2\theta}{n_o^2} \right]^{-1/2} \qquad 2.14$$

For a negatively birefringent uniaxial crystal as e.g., lithiumniobate, $LiNbO_3$ $n_e \leq n_e(\theta) \leq n_o$, (for a positive uniaxial crystal $n_o \leq n_e(\theta) \leq n_e$). In the case of SHG the two types of BPM is achieved by choosing a propagation direction such as:

	Negative uniaxial	Positive uniaxial
Type I	$n_e(2\omega,\theta) = n_o(\omega)$	$n_e(\omega,\theta) = n_o(2\omega)$
Type II	$n_e(2\omega,\theta) = (n_o(\omega)+n_e(\omega,\theta))/2$	$n_o(2\omega) = (n_e(\omega,\theta)+n_o(\omega))/2$

Table 2.1 Relations between the refractive indices for birefringent phasmatching (SHG).

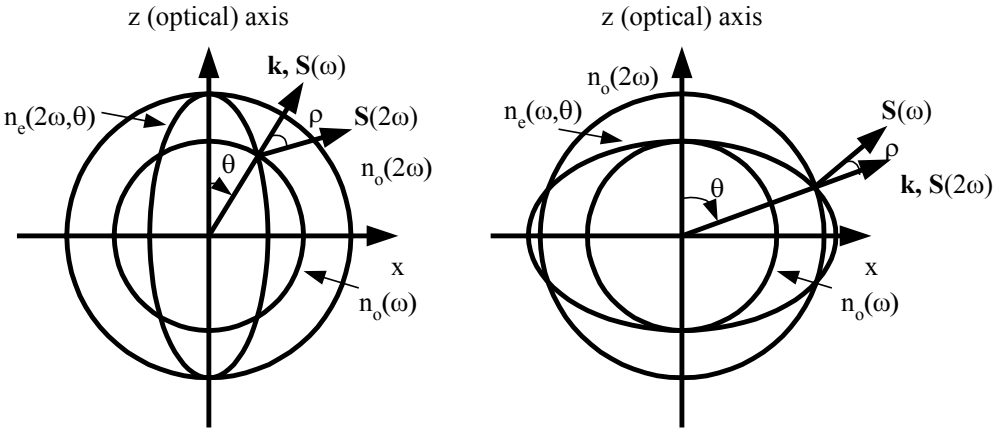

Fig 2.3 Type I phasematching in a negative and positive uniaxial crystal respectively.

It is possible to graphically find the proper phasematching angle for type I SHG by plotting the index surfaces, see Figure 2.3. If the phasematching is critical i.e., $\theta \neq$

90°, the direction of the power flow for the extraordinary wave given by the Poynting vector[11] **S** = **E**×**H** and the wavevector will differ with an angle ρ, since the Poynting vector always is normal to the index ellipsoid, **H** is the magnetic field. ρ is given by:

$$\tan\rho = \tfrac{1}{2} n_e^2(\theta)\left[\frac{1}{n_e^2} - \frac{1}{n_o^2}\right]\sin 2\theta \qquad 2.15$$

The walk-off angle $\rho \approx 2°$ at $\theta = 45°$ for typical birefringent crystals. After a distance L_a called the aperture distance the ordinary and extraordinary waves have separated completely and do not interact any longer:

$$L_a = \frac{\sqrt{\pi} w_0}{\rho} \qquad 2.16$$

The situation for biaxial material where $n_x \neq n_y \neq n_z$ are somewhat more complicated, but it has been treated in detail by Hobden[12].

It is now clear that BPM possess some inherent disadvantages. First of all as mentioned above the interacting waves will walk-off from each other if the conversion process is critically phasematched and hence the effective interaction length will be limited. (For a beam radius of 100 μm and $\rho = 2°$ the aperture length will be ~5 mm). The wavelength region that is possible to phasematch is usually also limited, since the material might lack sufficient birefringence over wide parts of its transparency range. Furthermore, the chosen propagation direction also affects the effective nonlinear tensor element, typically for the worse[3]. Another aspect to be considered for BPM is the acceptance angle, Δθ. $\Delta k \neq 0$ if the propagation direction of the pump wave deviates by a small amount from the optimum phasematching direction given by the angle θ. Δθ is the angle between these two directions and formulas for its calculation is given in ref. [13] for the different types of angle phasematching. Non-critical phasematching is once again the preferred type, since it provides the largest acceptance angle.

Other possibilities to obtain phasematching is by using waveguide dispersion or to periodically manipulate the material to reset the phase difference between the interacting fields after every coherence length and hence achieve phasematching on the average over the entire crystal length.

3 Quasi-phasematching

3.1 Theory

The technique of quasi-phasematching, QPM, was proposed already in the early 60's when the field of nonlinear optics had just emerged[10,14]. The idea is to correct for the phase-mismatch between the interacting fields at regular intervals by imposing a periodic structure to the material. Now, consider second harmonic generation once again. If the process is not phasematched, the energy will after the first coherence length in the crystal start to flow back from the generated field to the incident and after $2L_c$ the generated field is back to zero energy. This energy fluctuation is repeated with a period of $2L_c$ and the generated wave will not grow with distance. This case is illustrated in figure 3.1, "line (c)".

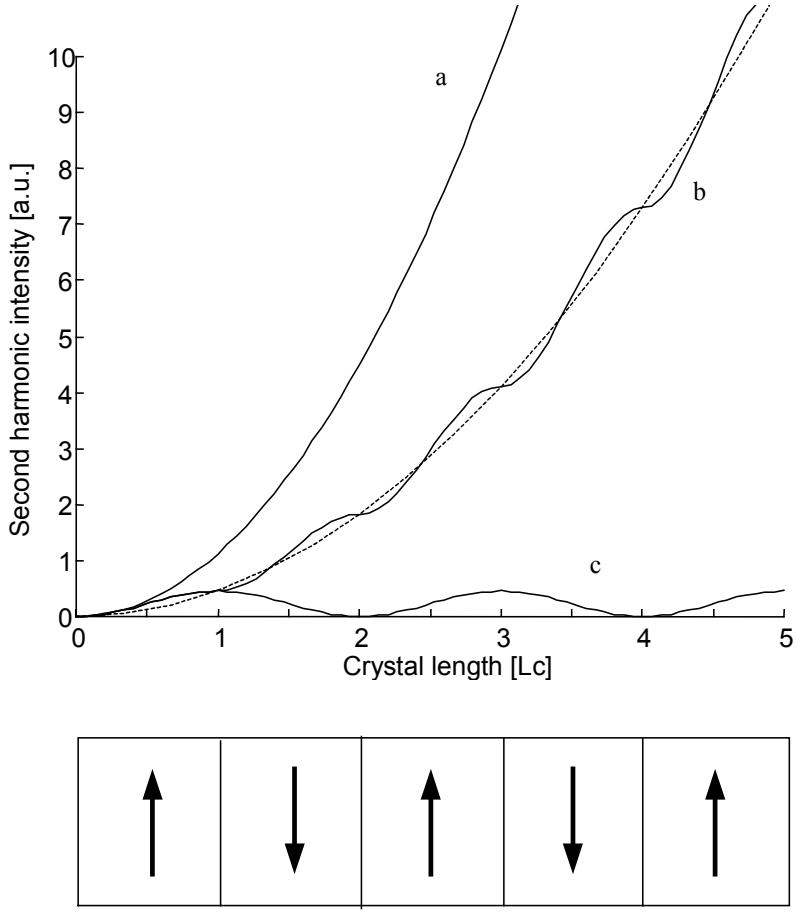

Fig. 3.1 Second harmonic generation in a material with different phasematching conditions. Line (a): Perfect phasematching, $\Delta k=0$, througout the entire crystal. Line (b): First order quasi-phasematching in a crystal where the spontaneous polarisation is reversed every coherence length. Line (c): The material has a constant phase-mismatch. The dotted line is "line (a)" multiplied by the appropriate factor $(2/\pi)^2$ for first order QPM.

However, if the phase-mismatch is put to zero after every coherence length, the energy will continue to flow from the incident waves to the generated one without

interruption. One way to attain the desired periodic phase-reset is to modulate the relevant nonlinear tensor element of the process. The most rapid growth of the generated field will occur if the sign of d_{ijk} is reversed every coherence length, the QPM is said to be of the first order. The output wave will then grow in a stepwise fashion as in figure 3.1, "line (b)". Figure 3 also display the case of perfect phasematching, "line (a)", this corresponds to equation 2.11 with $\Delta k = 0$ and the frequency doubled intensity is proportional to the square of the crystal length.

The needed sign modulation of d_{ijk} to achieve QPM can be accomplished by periodically inverting the spontaneous polarisation, P_s, of the ferroelectric crystal. Assume now that this inversion can be described by a function g(x), which is a rectangular function with the period Λ and magnitude +/-1. Since g(x) is a periodic function it can be expanded in its Fourier series:

$$g(x) = \sum_{m=-\infty}^{\infty} G_m \exp(iK_m x) \qquad 3.1$$

K_m is the magnitude of the grating vector, $\mathbf{K}_m$. The direction of the grating vector is normal to the grating i.e. along the propagation direction x of the electromagnetic waves.

$$K_m = \frac{2\pi m}{\Lambda} \qquad 3.2$$

The Fourier series in equation 3.1 can be inserted into the second equation of the equation system 2.10 to reveal how the growth of the harmonic field is affected by the inverted structure[15].

$$E_{2\omega} = \frac{i\omega}{n_{2\omega}c} d_{ijk} E_\omega^2 \int_0^L \sum_{m=-\infty}^{\infty} G_m \exp(i(K_m - \Delta k)x)dx \qquad 3.3$$

The conversion can only be efficient if $\Delta k_{tot} = \Delta k - 2\pi m/\Lambda \approx 0$, which is fulfilled for just one term in the series of g(x). This statement can be extended to hold for all second order nonlinear mixing processes. As seen in figure 3.1 and from equation 3.3 there is a price to be paid for QPM. The effective nonlinear coefficient for QPM is reduced to $d_{eff} = G_m d_{ijk}$. For a rectangular structure with a duty-cycle, $D = L_p/\Lambda$, where L_p is the length of the grating that have a positive sign of its d_{ijk}, the coefficient G_m takes the following values:

$$G_m = \frac{2}{\pi m}\sin(\pi m D) \qquad 3.4$$

The optimum QPM grating has a 50 % duty-cycle and m = 1, i.e., the period $\Lambda = 2L_c$ and $d_{eff} = 2d_{ijk}/\pi$. However, since the variable m can take all integer values, more than one frequency conversion process can be phasematched at the same time for the same grating. These extra processes can in principal limit the efficiency of the wanted nonlinear phenomena, although the value of the nonlinear coefficient drops rather fast for high order QPM. If the duty-cycle deviates with a small amount from 50% even

orders of QPM can also be seen [II], [III]. The absolute value of the normalised effective nonlinear coefficient d_{eff} versus duty-cycle for the sixth order QPM is plotted in figure 3.2.

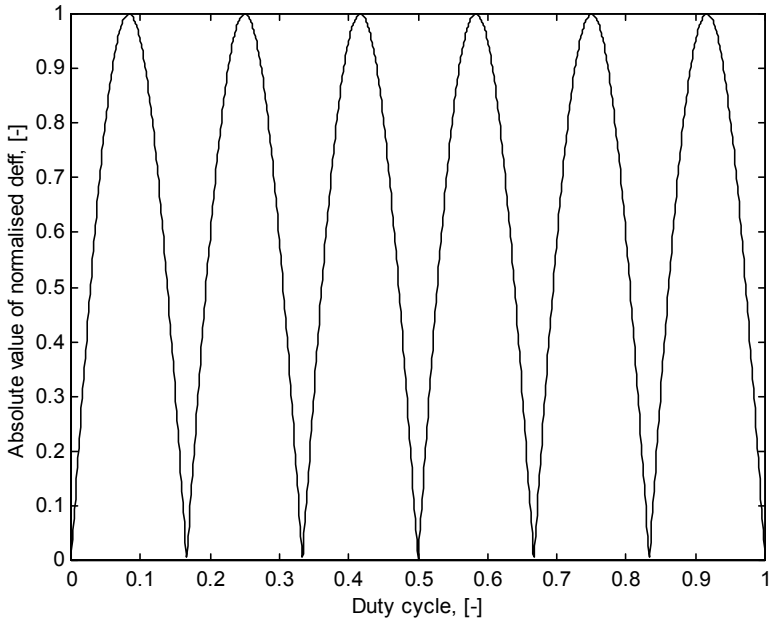

Fig. 3.2 Absolute value of normalised d_{eff} versus duty-cycle for 6th-order QPM.

3.2 Techniques to implement quasi-phasematched structures

Different techniques for the implementation of QPM structures have been proposed and demonstrated over the years. One of the first methods was the stacking of thin wafers of the nonlinear material, where every other wafer is rotated 180° relative to the one before. This was tested 1963 by Franken and Ward[14] using a stack of rotated quartz plates. A considerable drawback with this method is that the many wafer surfaces in the stack is causing large reflection losses. To circumvent this problem Gordon *et al*.[16] suggested that the wafers could be diffusion-bonded together to reduce the reflection losses. Several groups have later demonstrated this both for SHG and DFG in GaAs[17,18]. Levine *et al*. have demonstrated SHG in a waveguide filled with liquid nitrobenzene[19]. A periodic electrode was used to receive the necessary inversion of the nonlinear coefficient in the liquid. It has also been suggested to launch the interacting waves into the nonlinear crystal at an angle. The waves will then bounce back and forth in a zig-zag pattern when they propagate inside the material and the phaseshift that is received from total internal reflection will make up for the phase-mismatch accumulated over distance[10].

When it comes to ferroelectric materials there are several possible ways to achieve the desired domain inversion, i.e. the periodic reversal of the direction of the spontaneous polarisation.

One technique is to directly reverse P_s periodically during crystal growth. It has been demonstrated for example in $LiNbO_3$, that yttrium-doping during growth by the

Czochralski method can accomplish this. A first order periodic domain structure for blue light generation has been fabricated using this technique[20].

It is also possible to use the in- or outdiffusion of ions in planar waveguides to produce QPM gratings. Ti-indiffusion was used to fabricate a 7 mm long domain inverted channel waveguide in $LiNbO_3$ for first order SHG QPM[21]. In potassium titanyl phosphate, $KTiOPO_4$, was the polarisation inversion done by an exchange of Rb^+ and Ba^{2+} ions. When $KTiOPO_4$ is immersed in a salt bath containing $RbNO_3$ and $Ba(NO_3)_2$ an exchange of Rb^+ and K^+ ions will occur. At the same time the Ba^{2+} ions will cause domain inversion on the original c^- side of the crystal. (The surface of the material from which the Ps vector is pointing is denoted the c^- side). QPM waveguides have been fabricated through Rb/Ba ion-exchange in both hydrothermal and flux grown $KTiOPO_4$ crystals[22,23].

A third method is to induce the space-charge field necessary for domain reversal by electron injection into the crystal at the c^- polar surface. Electron beam writing has been used to write periodic patterns through 1 mm thick hydrothermal $KTiOPO_4$ for fifth order SHG[24], as well as in half millimetre thick lithium tantalate, $LiTaO_3$ and $LiNbO_3$ samples[25,26]. However, with this poling process it is difficult to get a perfect duty-cycle through the entire thickness of the crystals, due to the lateral spreading of the domains.

The most widely used and efficient way to fabricate periodic domain structures today is by electric field poling. The method has made it possible to scale up the periodically poled volumes in the crystals considerably. It has also turned periodic poling into a more flexible process and increased the reproducibility. To implement the domain inversion, periodic electrodes are deposited on one or both polar surfaces of the ferroelectric crystal by lithographic techniques. A strong external electric field is then applied over the sample to reverse the spontaneous polarisation underneath the contact areas of the electrodes. Yamada *et al*.[27] was the first to demonstrate electric field poling of bulk $LiNbO_3$ in 1993. Since then intensive research work performed by several research groups around the world has turned periodic electric field poling into a mature technology with commercial production. To mention just a few references: Webjörn[28], Miller[29] and Myers[30] have worked with periodically poled $LiNbO_3$ (PPLN), Karlsson[31], Chen[32] and Rosenman[33] with periodically poled $KTiOPO_4$ (PPKTP) and its isomorphs, and Meyn[34] with the periodic poling of potassium niobate, $KNbO_3$ (PPKN).

In this thesis, QPM devices for optical parametric oscillation and amplification have been fabricated by electric field poling of flux grown $KTiOPO_4$. A monitoring method to view the inversion of the ferroelectric domains during periodic poling in situ and in real-time has also been developed [IV].

3.3 Advantages of quasi-phasematching

Above, it was discussed that QPM gives a penalty in form of a reduction of the nonlinear coefficient for the frequency conversion process. However, the benefits of QPM are several and they compensate this disadvantage more than enough. First of all, QPM gives the opportunity to have all the interacting waves polarised in the same

direction. It is then possible to utilise the largest nonlinear tensor element of the particular material, which often is an element with both indices equal d_{ij}, i = j. For example, d_{33} is the largest tensor element for $LiNbO_3$, $LiTaO_3$, $KNbO_3$ and for $KTiOPO_4$ and its isomorphs. Additionally, Poynting vector walk-off between the fields can be avoided, since all fields can be polarised parallel to one of the principal axes, e.g. the z-axis. Because of these two facts, a multitude of efficient devices for frequency conversion have been demonstrated in periodically poled materials, as shown in this thesis work and by many other researchers as well.

Furthermore, phasematching can be achieved over the entire transparency range of the material, since the momentum equation now can be engineered. In the specific case of parametric down conversion this leads to the fact that virtually any pair of signal and idler photons can be produced from the pump photon as long as the energy before and after the conversion is conserved. This is illustrated in figure 3.3 for four different pump wavelengths in PPKTP.

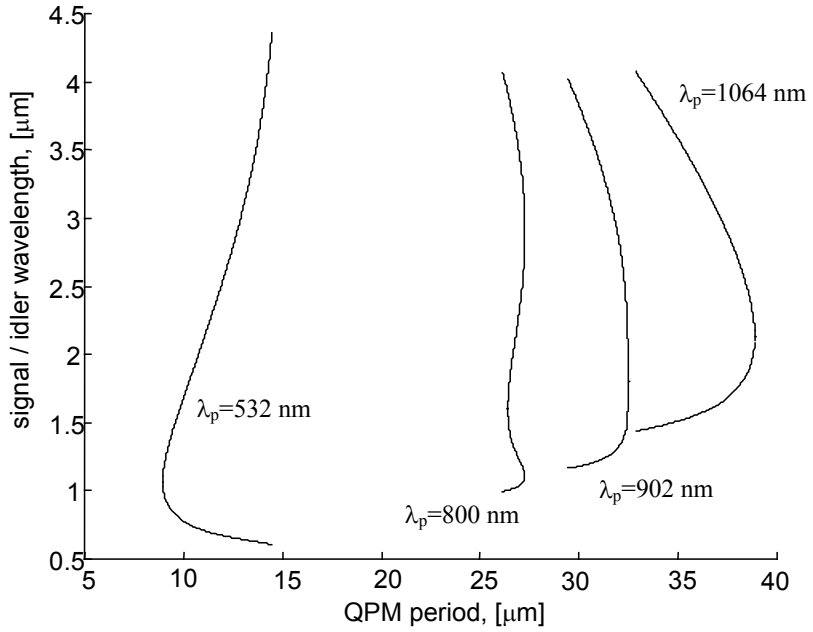

Fig. 3.3 Variation in output wavelengths versus QPM grating period Λ, for four different pump lasers.

The phasematching bandwidth will be particularly wide, when the second derivative of the refractive index approaches zero, as seen in figure 3.3, for the pump wavelength of 902 nm. This can be advantageous for the generation of femtosecond pulses[35]. For some shorter pump wavelengths the tuning curve will also exhibit retracing behaviours, i.e., more than one pair of signal / idler photons might be phasematched simultaneously, as seen for λ_p = 800 nm. Figure 3.3 also shows that the grating periods used for PPKTP OPOs, which are pump by Nd:YAG lasers at 1.064 μm, span approximately from 33 μm to 39 μm and that shorter grating periods are used for the visible part of the spectrum. The shortest grating periods are used for frequency doubling to the blue and ultraviolet spectral regions. Periods as short as 2.95 μm have been poled in $KTiOPO_4$ for SHG to 390 nm [36]. However, it might be difficult to pole large areas of high quality with fine pitch gratings. Type II QPM might then be

the solution, i.e., to pump with two orthogonal polarisations, since this leads to longer periods for SHG [AI].

QPM provides a great flexibility in the design of second order nonlinear devices and highly sophisticated grating structures can be implemented in the material. For example, the signal / idler tuning ranges of OPOs can be enhanced by placing several gratings beside each other. Up to 25 gratings have been fabricated in PPLN[37]. Fan-shaped gratings have been tried for the same reason[38,39]. Different grating periods can as well be applied in sequence to support cascaded up-conversion (or down-conversion) for frequency-metrology applications[18]. Crystals that possess a lateral variation in the length of the grating can be used to shape the output beam spatially[40].

Furthermore, the grating period does not have to be constant over the entire crystal length. Linearly chirped gratings, i.e. the period increases or decreases linearly with distance, provide additional possibilities e.g. compression of ultrashort pulses through frequency conversion. The idea is to frequency convert the spectral components of the incoming pulse at different positions in the crystal to make up for the difference in group velocities between the incident and generated pulses[41,42]. The gain bandwidth will broaden substantially for chirped gratings and the peak efficiency will drop. In figure 3.4 the gain bandwidth for frequency doubling from 1.064 μm in a 10 mm long PPKTP crystal is plotted versus pump wavelength. In case (a): Λ = 8.99 μm is constant. For the chirped grating, (b), the period varies from 8.96 μm to 9.02 μm.

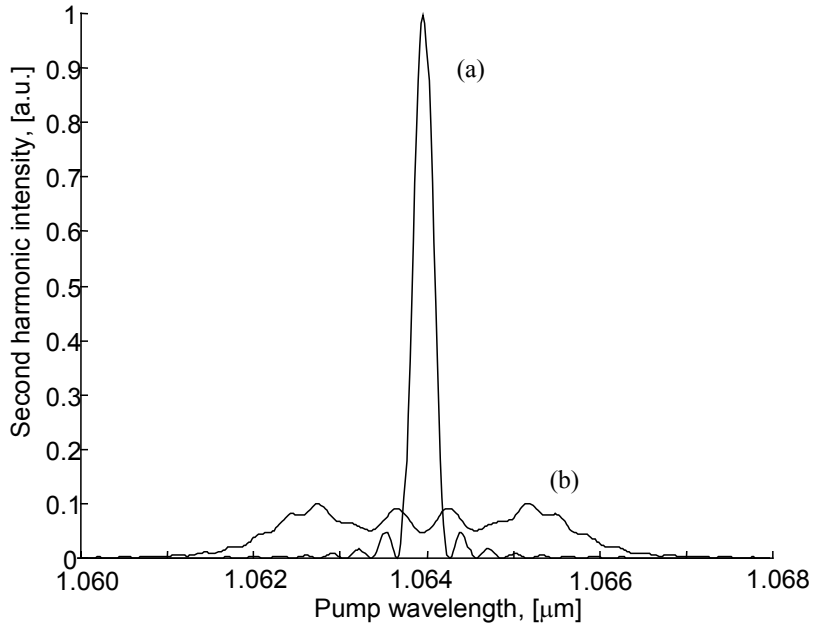

Fig. 3.4 Second harmonic gain bandwidth for a 10 mm long PPKTP crystal pumped at 1.064 μm. (a): The grating has a uniform period, Λ = 8.99 μm. (b): The chirped grating period varies, Λ = 8.96-9.02 μm.

In principle, it is the lithographic technique that limits the shape of the pattern that can be fabricated in the material. A 2-dimensional hexagonal structure for SHG in a $LiNbO_3$ crystal has been implemented by electric field poling[43].

3.4 Disadvantages of quasi-phase matching

In fact, there are not many disadvantages with QPM. The extra processing steps that are needed to fabricate the gratings are time consuming and will of course add cost. Defects in the gratings that are introduced during the lithographic process or during poling will affect the conversion efficiency in a negative direction and might also affect the gain bandwidth. Possible defects can for example be missing domains, constant or random errors of the QPM period and duty-cycle errors. Several authors have investigated these problems[15,44-46]. Another negative aspect is that high-order quasi-phasematched interactions may affect the studied conversion process. Such parasitic processes of various efficiencies have been observed in several experiments during this research work [II, III, VI, VIII]. Most of them have been very weak and they have left the studied mixing phenomena more or less unchanged. Finally, the reduction of the nonlinear coefficient through the G_m coefficient may be regarded as a drawback.

However, the benefits, which QPM provide are by far greater than these disadvantages. This statement is in my opinion, supported by the results from the research work presented in this thesis.

4 Potassium titanyl phosphate

4.1 Introduction

Potassium titanyl phosphate, $KTiOPO_4$ (KTP), does not exist naturally. It was synthesised for the first time in 1890 [47]. After that it seems like the material was more or less forgotten until the 1970s when the crystal got new attention. Tordjman *et al*. analysed the crystal structure in detail in 1974, [48] and in 1976 researcher at DuPont Inc., USA, started to investigate KTP's nonlinear optical as well as its mechanical properties[49]. KTP possess a high nonlinear susceptibility, it has a high resistant to optical and mechanical damage, and its transparency range extends from the ultraviolet to the end of the mid-infrared part of the spectrum. Other important features for nonlinear optics are that the crystal has enough birefringence for BPM and that KTP is ferroelectric, which gives the opportunity to periodically pole the material. The material can also be purchased from several vendors around the world, which lowers the cost of the material. This combination of properties makes KTP a good candidate as nonlinear crystal in frequency conversion devices.

4.2 Crystal structure

The crystal structure of KTP and its isomorphs is orthorhombic with the acentric point group *mm2*, and space group $Pna2_1$. The principal axes x, y, z correspond to the crystallographic directions a, b, c of the crystal, c being the polar axis, following the conventional labelling in the literature[50,51]. The KTP structure[48,49,52] is composed of chains of TiO_6 octahedra, which are linked at two corners and separated by PO_4 tetrahedra. There are four asymmetric units with two formula units of $KTiOPO_4$, in each unit cell of the crystal. In these chains the Ti-O bonds are alternating long and short, and form a helical structure with alternating direction [0 1 1] and [0 $\bar{1}$ 1], each unit cell have two chains. In the case of KTP there are two types of cations' sites. One of the sites is 8-fold coordinated and the other is 9-fold coordinated. The K^+ ions are weakly bonded to both the octahedra and the tetrahedra. The crystal structure contains channels along the z-axis, as seen in figure 4.1.b. The cations can relatively easy diffuse in these channels and this leads to a diffusion constant several orders of magnitude greater in the z-direction compared to the x or y directions.

For the other KTP isomorphs the formula unit is written $MTiOXO_4$, where M can be substituted for K, Rb, Cs, Tl or NH_4 and X can be either P or As. It should be noted though that CTP has a cubic structure of pyrochlore type[53] and that it is foremost KTP, KTA, RTA, and RTP that are used in optical experiments.

The literature is not entirely consistent in determining which bonds in the KTP crystal structure that contributes the most to the optical nonlinearity. Zumsteg *et al*.[49] came to the conclusion that it is the short Ti – O bonds in the helical chain that is the major contributors and that the other Ti – O bonds as well as the PO_4 and K – O groups are less prominent. On the other hand Xue and Zhang[54] came to the opposite conclusion, i. e. according to them it is the PO_4 tetrahedra and the K – O groups that primarily causes the nonlinearity.

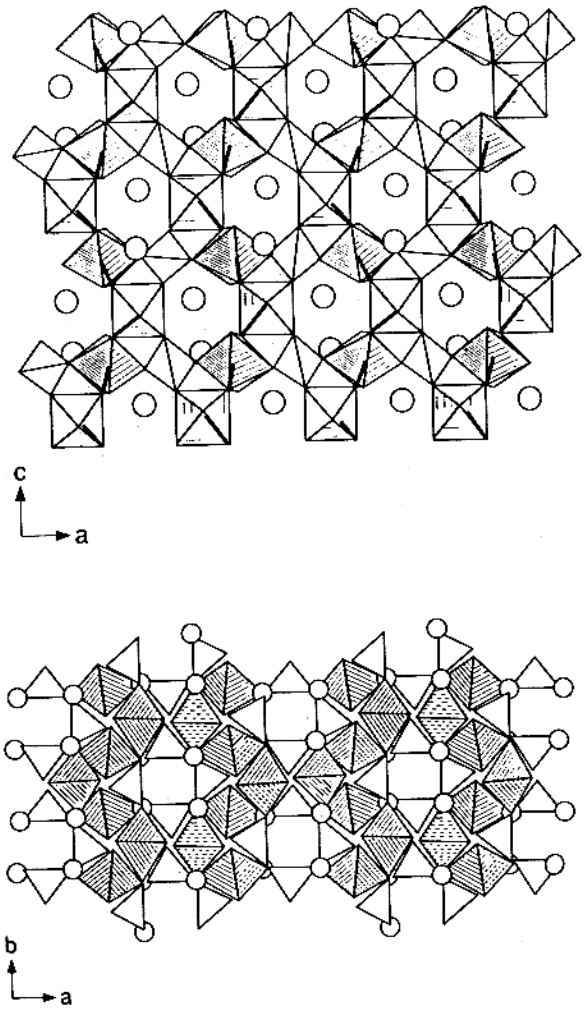

Fig. 4.1 (a): The KTP crystal structure projected in the a–c plane. (b) The KTP crystal structure projected in the a–b plane. The open circles are K ions, the PO_4 tetrahedra are open elements and the TiO_6 octahedra are shaded. The bold lines symbolise the short Ti – O bonds[52].

4.3 Growth techniques for members of the $KTiOPO_4$ family

There are mainly two methods for growing KTP isomorphs. In the first, the crystals are grown from a solvent that contains the dissolved components necessary to form the crystal. The solvent is called a flux and has given name to the process, flux growth. If the solvent only contains the material which constitutes the crystal it is named a self-flux. The self-flux is kept in Pt-containers at high temperatures (800 - 950 °C) and the growth starts in the supersaturated melt and continues during cooling. The stability of the temperature is an important issue for this process. It should be better than +/- 0.05 K [55] at the crystal position otherwise flux inclusions and growth striations might appear. Cheng *et al*. have synthesised KTP, KTA, RTA, RTP and CTA crystals using the method of self-flux growth[56]. The other method is called hydrothermal growth. Here the synthesis takes place in a container called autoclave at high temperatures and pressures, where aqueous solvents are used to dissolve and

recrystallize the material. Typical parameters for hydrothermal growth of KTP are temperatures of 400 – 500 °C and pressures of 1 – 2 kbar [57].

Growing KTP by a self-flux process is faster than using the hydrothermal technique. This leads to a better availability and approximately a 10 times lower price for flux KTP compared to hydrothermal KTP.

4.4 Conductivity of $KTiOPO_4$

Hydrothermal and flux grown KTP have very similar mechanical and optical properties. One exception though is their dielectric properties, which are very different. The conductivity along the z-axis can vary up to four orders of magnitude as illustrated in figure 4.2 [52], depending on which growth process that was employed. The complex permittivity, ε_c, is normally defined as $\varepsilon_c = \varepsilon' - i\varepsilon'' = \varepsilon_r\varepsilon_0 - i\sigma/2\pi f$ [11], where ε'' takes into account the losses of the material. Bierlein *et al*. have the following definition $\varepsilon = \varepsilon_c/\varepsilon_0$ [52] in the graph reproduced in figure 4.2.

$$\begin{aligned} \varepsilon_{rz} &= \varepsilon'_{33} \\ \sigma_z &= 2\pi f \varepsilon_0 \varepsilon''_{33} \end{aligned} \qquad 4.1$$

Here ε_{rz} and σ_z are the relative dielectric permittivity and the conductivity along the z-axis respectively and the frequency is f.

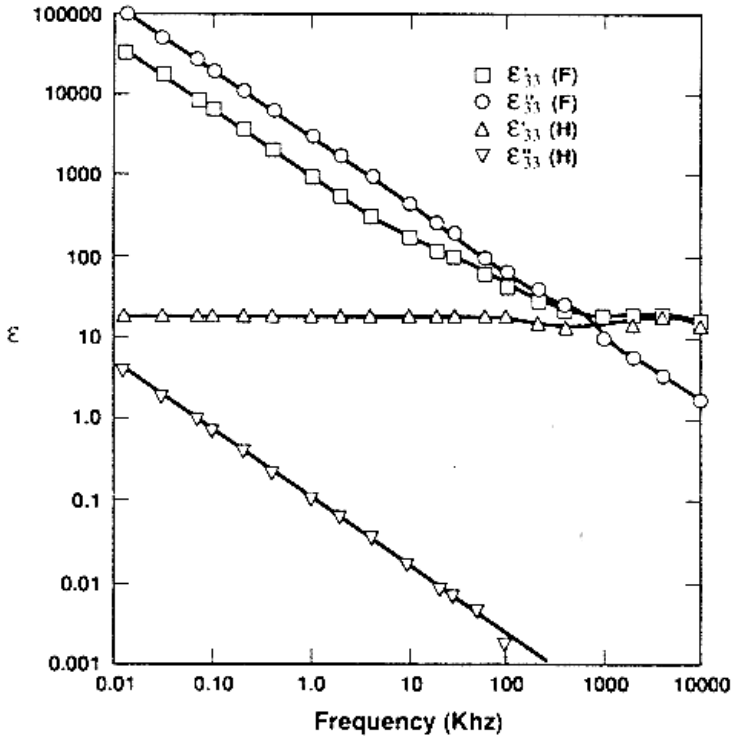

Fig. 4.2 Frequency dependence of dielectric constants along the z-axis for flux grown (F) and hydrothermally grown (H) KTP[52].

The reason for this discrepancy between flux grown and hydrothermally grown material is that the conductivity, to the largest extent, is governed by the K ions moving in the channels parallel to the z-axis through a vacancy transport mechanism, i.e. the cations are hopping between vacant sites in the lattice. Hydrothermally grown KTP crystals have a lower number of vacancies, probably due to the lower growth temperature, and hence possess a lower ionic conductivity than flux KTP. The anisotropy of the crystal structure impose a great difference, three to four orders of magnitude, in the conductivity along the principal axes of KTP[50,58]. σ_z is also varying significantly between the different members of the KTP family. The Rb ions have a lower mobility in the lattice, since they are bigger than the K ions and this result in a lower conductivity for RTP and RTA compared to KTP.

In this research work periodically poled flux grown KTP has been studied as gain material in optical parametric oscillators and amplifiers. Therefore, I will in the following only refer to KTP and drop the specification of the growth technique. Flux grown RTA was used as a comparison in one paper [VII].

4.5 Ferroelectrics

KTP is a ferroelectric crystal with the c-axis as the polar axis. A crystal is said to be in its ferroelectric state, when the centre of positive charge does not coincide with the centre of negative charge for the unit cell, also when no external electric field is applied. The spontaneous polarisation, P_s, is then defined as the sum of all the individual dipole moments per unit volume[59]. Ferroelectricity usually disappears above a certain transition temperature called the Curie point, T_c, the material then becomes paraelectric. T_c = 936 °C for KTP[60]. The spontaneous polarisation causes a depolarisation field E_d to appear in the material. This field in turn is neutralised by mobile charge carries that can move to the surfaces of the crystal[61]. A plot of the spontaneous polarisation versus electric field for the ferroelectric state shows a hysteresis loop more or less centred on origo. The coercive field of the crystal is defined as the electric field necessary to invert the direction of P_s, i.e. the point(s) where the hysteresis loop crosses the electric field axis[61].

Regions in a ferroelectric crystal, which have identical direction of its spontaneous polarisation, are called domains. Clearly, it is important that the crystals used in nonlinear optics are single-domain before the periodic poling otherwise the efficiency of the process will be reduced. If this is not the case, a uniform poling can be applied to make the material single-domain before the implementation of the QPM grating. The thin region between opposite domains is called a domain-wall. The anisotropy of the crystal lattice of KTP makes domain-walls parallel to the plane [1 0 0] most likely, since these planes do not cut through the helical chains[60]. For other directions is the domain-wall energy considerably higher. In other words, the grating vector, $\mathbf{K}_m$, should be parallel to the x-axis in order to create a QPM structure of high quality in KTP[62]. Domains of opposite direction differ in signs of every polar property of any odd-rank tensor[58]. As a consequence of this, the d-coefficients on either side of a domain-wall will have opposite signs, since d_{ijk} has rank 3.

The spontaneous polarisation in KTP and isomorphs is sensitive both to pressure and temperature, i.e. the crystals are both piezoelectric[63] and pyroelectric[52].

4.6 Optical properties of $KTiOPO_4$

KTP is a biaxial crystal, i.e. the refractive indices for the principal axes of the material are all different, $n_x \neq n_y \neq n_z$. In the research described in this thesis the electromagnetic waves have almost always been polarised along the z-axis and hence n_z has been the refractive index to consider. Several dispersion relations, $n_z(\lambda)$, in the form of Sellmeier equations have been published for KTP and they all have contained considerable errors above approximately 2 μm wavelength. The situation improved recently when Fradkin-Kashi *et al*. published refined Sellmeier equations for KTP[64], as well as for KTA[65] and RTA[66]. They give a very small deviation between the calculated and the actual grating periods for parametric interactions in the infrared spectral region as shown in paper [VII]. Fan *et al.*, has reported very accurate dispersion relations for all three refractive indices in KTP for wavelengths shorter than 1.064 μm [67]. The Sellmeier equations can be written on the form:

$$n_z^2(\lambda) = A + \frac{B}{1-\frac{C}{\lambda^2}} + \frac{D}{1-\frac{E}{\lambda^2}} - F\lambda^2 \qquad 4.2$$

(The wavelength λ should be in μm).

	A [-]	B [-]	C [μm^2]	D [-]	E [μm^2]	F [μm^{-2}]
KTP[64],>1μm	2.12725	1.18431	0.0514852	0.6603	100.00507	0.00968956
KTA[65]	1.214331	2.225328	0.0318772	0.310017	80.820064	0.009381
RTA[66]	2.182064	1.307519	0.0520953	0.354743	81.197382	0.008921
RTP[68]	2.77339	0.63961	0.08151	0	0	0.02237
KTP[67],<1μm	2.25411	1.06543	0.05486	0	0	0.02140

Tabel 4.1 Sellmeier coefficients for equation (4.2) for KTP, KTA, RTA and RTP.

The output wavelengths from OPOs are often tuned by altering the temperature of the material. In order to predict the tuning rate it is important to have the correct value of the temperature derivative of the refractive index, dn/dT, as well as the expansion coefficient of the material[63], since the temperature also affects the grating period. The temperature dispersion is often presented in the form of a Laurent series:

$$\frac{dn_z}{dT} = \frac{p_1}{\lambda^3} + \frac{p_2}{\lambda^2} + \frac{p_3}{\lambda} + p_4 \qquad 4.3$$

(The wavelength λ should be in μm).
An alternative approach to this purely mathematical formula is to use the physical model developed by Ghosh[69].

$$2n_z \frac{dn_z}{dT} = GR + HR^2$$
$$R = \frac{\lambda^2}{\lambda^2 - \lambda_{ig}^2} \qquad 4.4$$

(The wavelength λ should be in μm).

p_j j = 1 - 4, are fitting parameters. λ_{ig} is the isentropic bandgap wavelength and the coefficients G and H are related to the thermal expansion coefficient and the so called excitonic bandgap of the material, respectively[69]. It is our experience that Wiechmann *et al.*[70] have published accurate thermo-optic coefficients, dn/dT, for KTP, when $\lambda \leq$ 1.064 μm. Ghosh is better for $\lambda >$ 1.064 μm. In the case of RTA, we have presented new parameters to further diminish the gap between calculated and experimental tuning data points of an OPO emiting around 1.6 and 3.3 μm [VII]. It should be noted though that an absolute value of dn/dT was not possible to derive with the used fitting procedure in paper [VII]. However, in the procedure to calculate an OPOs tuning rate the parameter p_4 is not necessary.

	p_1 [μm^3/ °C]	**p_2 [μm^2/ °C]**	**p_3 [μm/ °C]**	**p_4 [°C^{-1}]**
KTP[70], < 1 μm	12.415E-6	-44.414E-6	59.129E-6	-12.101E-6
RTA[VII]	0.1867E-6	13.2760E-6	-12.2556E-6	arbitrary value
	G [°C^{-1}]	**H [°C^{-1}]**	**λ_{ig} [μm]**	
KTP[69], > 1 μm	-7.4595E-6	52.9338E-6	0.279	
RTA [VII]	-9.8098E-6	52.5177E-6	0.3901	

Tabel 4.2 Coefficients for equation (4.3) and (4.4), for KTP and RTA.

Hansson *et al.*[71] have measured the transmission of KTP and its isomorphic compounds along all principal axes. However, in this work propagation of the waves along the x-axis have been desired for reasons described in paragraph 4.5. Figures 4.3 and 4.4 show transmission for KTP, KTA, RTP and RTA. All samples where 10 mm long except for the RTP sample which was 11.2 mm. The polarisation was along the z-axis.

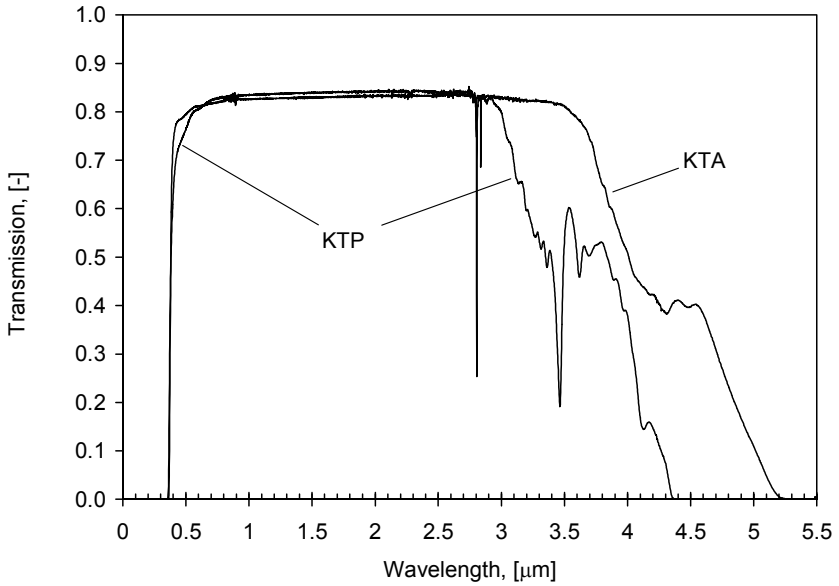

Fig. 4.3 Transmission window for KTP and KTA. No compensation for Fresnel losses was made[71].

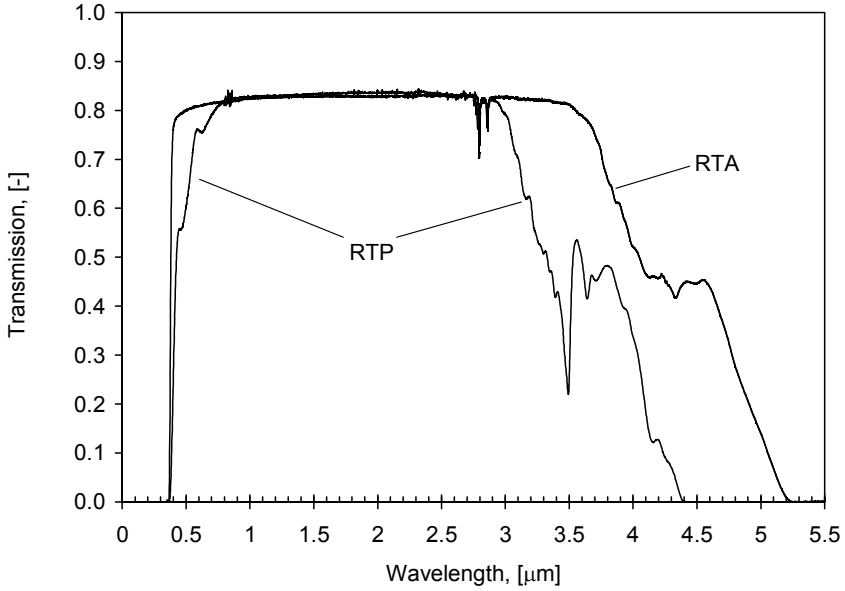

Fig 4.4 Transmission window for RTP and RTA. No compensation for Fresnel losses was made[71].

The ultraviolet cut-off wavelength varies from 0.365 μm in KTP to 0.393 μm in KTA for these measurements. In the infrared part of the spectrum the band-edge is at approximately 5.2 μm for the arsenate compounds and at 4.3 μm for the compounds containing phosphate. The increased absorption towards the long wavelengths is due to vibrations in the XO_4 tetrahedra. It is assumed that the heavier mass of As compared to P is the foremost reason for the increased transmission of the arsenate[71]. The absorption in the high transmission window is less than 0.6 %/cm for KTP[52]. The transmission dip close to 2.8 μm in the KTP isomorphs is caused by an OH^- group. Hydrogen gets trapped in the crystal structure during growth and becomes attached to an oxygen site. This pair of ions is then oscillating as a hydroxal molecule. This enhanced absorption at 2.8 μm was observed in the PPKTP OPO in paper [II], however high conversion efficiency was still possible to attain for that particular device.

The crystal symmetry of the KTP compounds give only five non-zero nonlinear optical coefficients. The non-zero d-coefficients are tabulated in table 4.3 and were measured at 1.064 μm by Cheng *et al.*[56], if not explicitly stated otherwise. The thermal expansion coefficients along the x-axis, α_x, are also given:

	d_{15} [pm/V]	d_{24} [pm/V]	d_{31} [pm/V]	d_{32} [pm/V]	d_{33} [pm/V]	α_x [°C^{-1}]
KTP	1.9 [57]	3.6 [57]	2.5	4.4	16.9	6.8E-6
KTA	2.3 [57]	3.2 [57]	2.8	4.2	16.2	7.0E-6
RTP	--	--	3.3	4.1	17.1	10.8E-6
RTA	--	--	2.3	3.8	15.8	15.1E-6

Table 4.3 Nonlinear optical coefficients and expansion coefficients for members of the KTP family.

The corresponding electro-optic coefficients measured at 0.633 μm [56] and the conductivity σ_z [72] for the KTP isomorphs are given in table 4.4.

	r_{51} [pm/V]	r_{42} [pm/V]	r_{13} [pm/V]	r_{23} [pm/V]	r_{33} [pm/V]	σ_z [S/cm]
KTP	7.3 [57]	9.3 [57]	9.5	15.7	36.3	$\sim 10^{-6}$-10^{-7}
KTA	--	--	11.5	15.4	37.5	$\sim 10^{-4}$-10^{-6}
RTP	--	--	10.9	15.0	33.0	$\sim 10^{-9}$
RTA	--	--	13.5	17.5	40.5	$\sim 10^{-8}$-10^{-9}

Table 4.4 Electro-optic and coefficients and conductivity along the z-axis for KTP and isomorphs.

Table 4.3 clearly shows that utilising d_{33} will be beneficial for the frequency conversion process in terms of efficiency and that the d_{33} coefficients have more or less the same values for all the compounds. In the process of deciding which isomorph from the KTP family to choose for a QPM mixing process issues like cost, homogeneity, size and availability of the non-poled wafers, as well as its conductivity and its transparency range must be taken into account. The conductivity plays a central role, since in general, it is easier to pole a material with low conductivity. It is foremost the four first issues above that have made KTP the preferred material in this thesis.

4.7 Optical induced damage in $KTiOPO_4$

It is necessary to use high pump field intensities in order for a frequency conversion process to be efficient and it is tempting to pump the device at higher and higher intensities. However, the risk of damaging the crystal increases with intensity and it is therefore important to know approximate damage thresholds of the material. It should here be emphasised that it is difficult to give a general value of the damage threshold of a material, since it varies with the average power, the pulse repetition rate, the pulse length, the spatial quality of the beam and the wavelengths of the pump and the generated light. The threshold might even vary between samples from the same compound although all other parameters are identical. This difference in threshold is probably due to variation of impurity levels during the crystal growth and other growth parameters.

The first optical damage mechanism to consider is direct optical induced breakdown of the crystal. The destruction of the material is caused by induced strain from high peak intensities via local temperature increase in the material. Damage may occur either inside or at the surface of the crystal. Optical coatings might affect the surface damage threshold negatively. In this thesis the most extensively used pump laser has been a flash-lamp pumped Nd:YAG laser with 20 Hz repetition rate, 5 ns pulse length and a beam quality factor M^2 >3. It has been possible to pump a KTP sample, used as gain medium in a parametric amplification process, without any observation of damage at peak intensities exceeding 900 MW/cm^2, [III]. For comparison, an early study of $LiNbO_3$ [73] indicated a damage fluency threshold of 2.7 J/cm^2, for 10 – 30 ns pulses. Extrapolating to 5 ns would give a peak intensity threshold of 540 MW/cm^2. However, the authors estimated a damage limit due to self-focusing of approximately 300 MW/cm^2 for $LiNbO_3$.

Another mechanism that limits the maximum pump intensities possible to use in nonlinear devices is the photorefractive effect[74]. The effect induces intensity dependent changes in the refractive index, which in turn causes beam distortions. For an OPO pumped in the infrared it is not the pump beam itself that causes the damage but the visible light from different parasitic process. The origin of the effect is that the visible light beams generate charge carriers from the material, which diffuse in opposite directions along the polar axis depending on their sign of charge. This process creates a space-charge field, which via the quadratic electro-optic effect affects the refractive index. It is well known that $LiNbO_3$ is sensitive to this type of damage, but it can be avoided by heating the crystal[75]. It has also been reported that PPLN should be less sensitive compared to non-poled $LiNbO_3$. A suggested explanation is that the charge carriers of the same kind will drift in opposite directions with the same spatial period as the period of QPM structure and the damage will diminish because of this imposed averaging effect on the phenomena[76]. KTP on the other hand is several orders of magnitude less susceptible to photorefractive damage than $LiNbO_3$, probably because of its higher conductivity[72], and it has not been observed in this study.

Photochromatic damage, so called grey-tracks, might also occur at high intensities. The grey-tracks are thin regions of darkening along the light beams in the crystal and it causes increased absorption at both infrared and visible wavelengths[77]. It is foremost shorter wavelengths that induce the effect[78] and it is attributed to the formation of colour centres involving Ti^{4+} and Fe^{3+} ions[79]. Heating the samples during operation reduces the risk of grey-track formation and may even make them disappear[80], [VIII]. The grey-tracks might also disappear over time[78]. The susceptibility for grey-track formation varies between different wafers of KTP, most likely due to differences in the conductivity and impurity concentrations[72]. Grey-tracks was observed in paper [VIII] and might have contributed to the reduced efficiency at the highest pump levels of the amplifier in paper [III].

5 Periodic electric field poling of $KTiOPO_4$

5.1 Introduction

It is a challenge to manufacture periodic domain inverted structures with high quality over large volumes in ferroelectric crystals. The dispersion of the materials sets the period of the grating to be on the order of $\Lambda = 3 – 40$ μm for optical frequencies, and for efficient high power nanosecond devices, crystal thickness of 1 – 3 mm are often desired. The duty-cycle has to be close to 50/50 over the entire length of the nonlinear material, which typically is 1-2 centimetres for the PPKTP OPOs presented here, to reach maximum conversion efficiency. Thus it is important to be able to carefully control and monitor the poling process, in order to implement QPM.

5.2 Domain switching of $KTiOPO_4$

To invert the direction of the spontaneous polarisation, P_s, and receive the required modulation of d_{33}, an electric field larger then the coercive field, E_c, of the material must be applied. In addition compensation charges Q must be provided, $Q = 2AP_s$, in order to balance the unscreened charges generated during the inversion. The area under which the polarisation is to be switched is denoted A. For periodic poling a metallic finger electrode and insulating photoresist between the fingers is deposited on one of the c-surfaces by a UV-lithographic technique, see figure 5.1. The insulation layer is thin enough to give a uniform electric field in the bulk of the crystal, but it is sufficiently thick to prevent charges supplied by the external circuit to be delivered to the region underneath[81]. It is believed that the mechanism of domain inversion in KTP is very similar to the one in $LiNbO_3$. It starts by nucleation of needle-like domains at the edges of the electrode, which propagate to the opposite side of the crystal, along the z-axis, and then merge in the x-y plane[30,82]. However, unlike $LiNbO_3$, KTP's strong anisotropic lattice structure reduces the domain growth in the x-direction[62]. As a consequence, the periodic electrode adhered to the crystal surface in this work has a 50/50 duty-cycle, figure 5.1, since the domain broadening under the insulated areas is assumed to be zero.

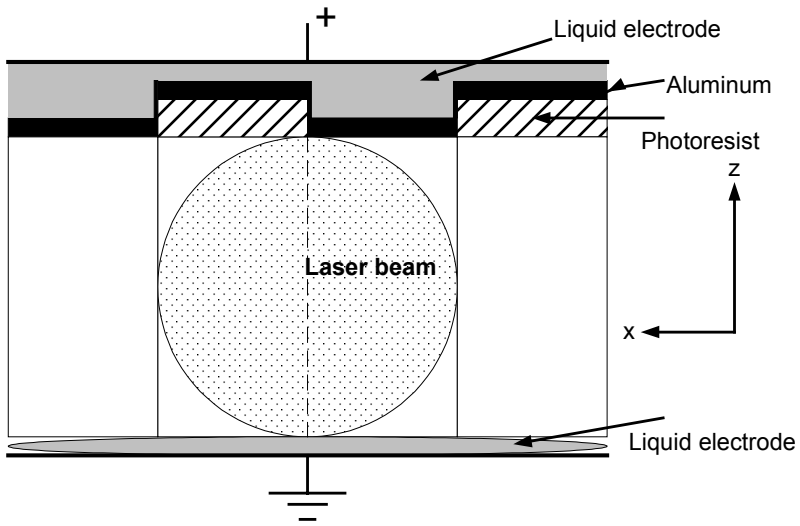

Fig. 5.1 Cross-section of the patterned crystal.

It has been proposed[60,83] that the physical reversal of the spontaneous polarisation in KTP takes place by a shift of the alkali ions in the –z direction, 9-coordinated K^+ ions become 8-coordinated and vice versa. Simultaneously, the short Ti-O bonds become long and the long ones short. The PO_4 tetrahedra and the TiO_6 octahedra undergo only a minor rotation. The result is that the structure has rotated 180°.

The high ionic conductivity along the polar axis of KTP makes the material somewhat difficult to pole. If the resistivity is low, a large current will flow through the sample when the high voltage is applied and dielectric breakdown might then occur in the crystal before the coercive field is overcome. To facilitate periodic electric field poling of flux grown KTP at room-temperature, Karlsson and Laurell[31,72] have developed a technique, where samples exhibiting a high conductivity are ion-exchanged in a Rb-melt to reduce the total conductivity of the material. This technique has been used in the work reported here. Another way of reducing the conductivity is to lower the temperature in order to freeze the ion migration in KTP[33]. KTP leaves its superionic state at $T \approx 170$ K, where the conductivity has dropped to $\sigma_z \approx 10^{-12}$ S/cm and has no frequency dependence any longer. A drawback with this technique is that the coercive field increases considerably at low temperatures, $E_c \approx 12$ kV/mm at 170 K, which makes the poling of thick crystals difficult.

5.3 Sample preparation and poling of $KTiOPO_4$

The flux grown KTP is bought in wafers of the approximate dimensions 30 x 30 mm^2 and varying thickness of 0.5 – 3 mm. The wafers are c-cut and the manufacturer has polished the c-faces. After arrival, the piezoelectric response and the conductivity of the wafers are mapped to determine the level of homogeneity of the material. If the material is found to be multi-domain, it is poled with uniform electrodes on both sides of the crystal (prepoled) to impose a single-domain structure.

The conductivity is measured by applying an electric pulse with an amplitude of 1.5 kV and duration of approximately 10 ms over the sample. The pulse shape resembles a square function and an equivalent frequency of 50 Hz for this half-cycle may be considered. The probed area has a radius of 0.5 mm. The conductivity varied between $1.3*10^{-7} \leq \sigma_z \leq 1.7*10^{-6}$ S/cm for the wafers I have poled. It was also found that the conductivity could vary up to a factor of 2 over the wafer area, probably due to inhomogeneities of the material in the number of vacancies and/or other impurities.

Wafers or part of wafers that exhibit high conductivity has been ion-exchanged in a 100 % $RbNO_3$ melt at 355 °C for approximately 2 hours. During the process the K^+ ions are exchanged for Rb^+ ions in the two thin layers closest to the c-faces of the crystal. The layer thickness is only a few micrometers. Since the Rb^+ ions are larger than the K^+ ions they have a smaller tendency to migrate through the lattice in the applied field and the resistivity will then increase in the ion-exchanged volume. This produces a voltage division between the exchanged layer and the bulk of the material, which has the same conductivity as before. This voltage division is beneficial for the poling process. The reason is that the regions close to the electrodes where the nucleation of the domains take place will experience a much stronger electric field for the same applied voltage if the ion-exchange has been performed. Hence the domain inversion is easier to initiate with ion-exchange than without. The total conductivity is

typically reduced a factor of 2 – 3 by this procedure. A layer of Aluminium might be deposited on one side of the material to inhibit the ion-exchange on that side. The idea is to have nucleation at only one electrode and receive a single direction of the domain growth.

After the ion-exchange the metal (if any) is removed and smaller samples are cut out from the wafers. The cuts are parallel to the principal axes and the final sample dimensions are typically 20 x 5 x 1 mm^3, (x,y,z), although other sample dimensions have been used, e.g. 12.5 x 12.5 x 0.5 mm^3 in paper [VI] or 10 x 5 x 3 mm^3 [II], [VII]. Subsequently, the faces that have been cut free are polished to optical quality to prepare for the monitoring methods. A photoresist (Shipley Microposit S1818) is spun on top of the sample, usually to a thickness of approximately 2 μm. The samples are baked in an oven at 100 °C for 30 min to harden the resist. Hereafter, the periodic pattern is inscribed in the resist by a standard lithographic technique. The grating vector is always parallel to the desired propagation direction, i.e. the x-axis. Following the development of the pattern, an approximately 0.1 μm thick aluminium layer is evaporated onto the crystal to form the finger electrode, as seen in figure 5.1, contact with the crystal surface is made every other half period. A metallic electrode has been applied here, since earlier research has found that the conductivity could be reduced up to 4 times with a metallic film on either side of the sample[72], as compared to applying liquid electrodes on both sides. The Al electrode does not have to be the periodic one. In the same study no further decrease of the total conductivity was detected, even though metal was used on both sides. The suggested explanation for the increased resisivity is that the film reduces the possibility for the K^+ ions to move between the crystal and the KCl solution that constitutes the liquid electrodes. Finally, the sample to be poled is mounted in a Plexiglas holder in the poling set-up. Electrical contact between the high-voltage supply and the sample's c-faces is provided by a nearly saturated solution of KCl. The periods used have been from 27.5 to 38.5 μm for the crystals I have fabricated and the metallic finger electrode has predominately been put on the c^+-side.

The poling is carried out by applying square-shaped electrical pulses with 1 – 10 ms duration, the rise time is less than 0.1 ms and the fall time is shorter than 1 ms for the pulse. The peak voltage of the pulse has to produce an electric field larger than the coercive field. Measurements have shown that the electric field necessary to start the domain reversal has varied approximately from 1.8 to 2.3 kV/mm over the samples used here. Short pulses are used in order to prevent an excess of energy to be delivered to the sample. Thermal effects could then damage the crystal. Another reason is to avoid unwanted internal bulk screening of the depolarisation field underneath the isolated half-periods of the crystal, which could lead to substantial domain broadening[81]. In paper [IV], it was measured that the relaxation time for the space-charge field induced during poling is on the order of 10^{-2} to 10^{-3} s for KTP at room-temperature.

5.4 Monitoring the poling process in $KTiOPO_4$ and its isomorphs

The progress of the domain inversion is monitored for every voltage pulse. The most common way to detect domain reversal in low conductive material such as $LiNbO_3$ is to measure the flow of compensation charges from the high-voltage supply to the sample during poling[30]. However, this method is very difficult to implement in flux grown KTP at room-temperature, since the high ionic conductivity along the z-axis makes it more or less impossible to discriminate between the poling current and ion-current through the sample. Instead Karlsson *et al*., have developed a monitoring technique for KTP and its isomorphic compounds that take advantage of the electro-optic effect[84]. A sketch of the poling set-up is given in figure 5.2.

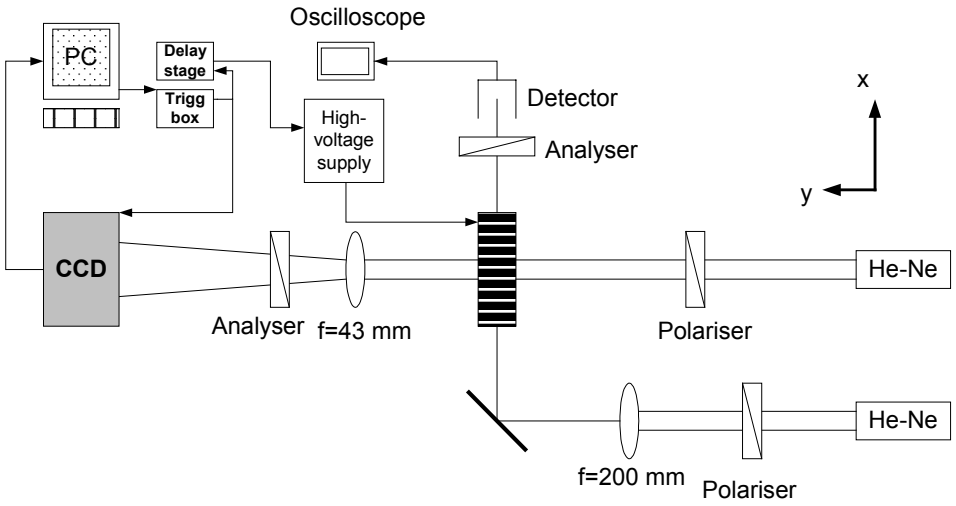

Fig. 5.2 Sketch of the poling set-up.

The idea behind the method is here briefly recaptured. The sample to be poled is mounted in the centre of the set-up and a He-Ne beam propagating along the x-axis is focussed into the sample. The beam is polarised 45° to the z-axis in the y-z plane. When the high voltage is applied over the sample it will affect the polarisation-state of the light and this is detected as an intensity change in the transmitted light by a second polarisation plate, a photodiode and an oscilloscope. If the applied electric field is weaker than E_c, the intensity will only be time-dependent during the rise and fall time of the pulse. When the applied field is larger than E_c, domains will be inverted during the pulse. This in turn will change the sign of the relevant electro-optic tensor elements and as a result, the polarisation-state will change even for a constant voltage. For the ideal case, when the sample has been poled with a perfect 50/50 duty-cycle, there will be no modulation of the intensity at the fall of the voltage pulse. Knowledge of how the poling proceeds are extracted from the intensity and voltage curves displayed on the oscilloscope.

5.5 A photographic method to monitor the domain inversion

It is important to constantly increase the knowledge of the poling process in order to improve the manufacturing procedure in terms of yield and quality. In this thesis work, a photographic method has been developed to monitor the inversion of the

ferroelectric domains *in situ* and in real-time [IV]. The method makes use of the electro-optic effect and a high-speed charge coupled device (CCD) camera. The high speed of the CCD camera gives the opportunity to observe the dynamics of the poling process, and to probe the samples afterwards to evaluate the QPM grating formed in the bulk.

The photographic monitoring method employ a beam from a He-Ne laser, which is polarised 45° towards the z-axis and is directed along the y-axis of the sample, figures 5.1 and 5.2. An analyser at -45°, is located after the exit surface and the CCD matrix detector measures the intensity of the transmitted light, i.e. the result is a two-dimensional map of the intensity in the x-z plane. The imaged area is approximately 350 x 350 μm^2, which corresponds to approximately 10 grating periods. A computer controls the operation of the CCD camera, which when set at maximum speed can register a new picture every 1.1 ms. Simultaneously, the computer also triggers the high-voltage switch, which delivers the electrical pulse to the KTP sample. A delay stage is needed to synchronise the two trigger pulses correctly.

The CCD camera is built up of 128 x 128 individual pixels. The intensity, I, at a specific pixel depends on the total phase shift, Γ, between the x and z components of the electric field in this part of the beam, accumulated during the propagation through the material. The phase retardation consists of two terms and is written:

$$\Gamma = \Gamma' + \Gamma'' = \frac{2\pi L_y}{\lambda_0}\left(n_z - n_x\right) + \frac{\pi L_E E_z}{\lambda_0}\left(n_x^3 r_{13} - n_z^3 r_{33}\right) \qquad 5.1$$

The propagation length along the y-axis is L_y, L_E is the distance affected by the electric field, E_z, λ_0 the wavelength and r_{13} and r_{33} are the relevant electro-optic tensor elements for the process. $L_E < L_y$ since the edges of the crystal holder limits the area of contact between the sample and the conducting liquid. If it is assumed that the sample is perfectly poled with a 50 % duty-cycle and $E_z < E_c$, the visibility, V, between two adjacent half periods is calculated to be:

$$V = \frac{I - I_{inv}}{I + I_{inv}} = \frac{\sin\Gamma' \sin\Gamma''}{1 - \cos\Gamma' \cos\Gamma''} \qquad 5.2$$

I_{inv} is the intensity from the inverted domain. This contrast provides a direct image of the QPM structure. In figure 5.3 the absolute value of the visibility for two neighbouring half periods is plotted versus the applied voltage. The parameters is for a KTP sample: λ_0=633 nm, n_x=1.7626, n_z=1.8655, L_y=5 mm, L_E=3.2 mm, the electro-optic coefficients are from table 4.4. In figure 5.3 it is seen that the visibility might be low or even zero although the sample has an ideal duty-cycle. It might then be necessary to apply another pulse at a different voltage, before any conclusion of the quality of the QPM structure can be drawn. Any intermediate stage of the poling process may also be seen as an intensity variation in the picture, provided that the CCD camera is fast enough to detect it.

The computer could register a maximum of 40 pictures per poling sequence. Nine pictures were taken during the 10 ms the high-voltage was applied. The time when the pulse was switched on was denoted τ_{p1} and the switch off time τ_{p2}. The visibility data

from the picture was obtained by extracting the intensity matrix behind each picture and calculating an average value for all 10 periods.

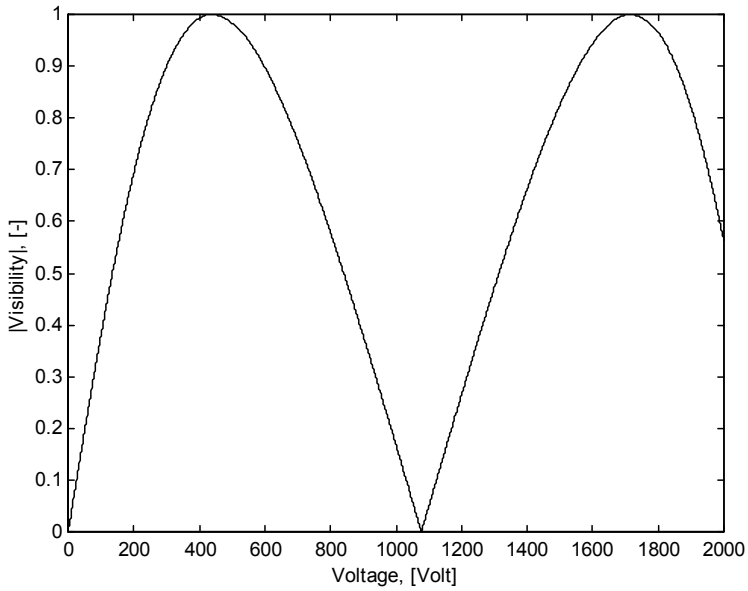

Fig. 5.3 The absolute value of the visibility versus applied voltage for two neighbouring half periods. The sample thickness is 1 mm.

A few pictures from a poling sequence is shown as an example in figure 5.3. The pictures were taken close to the original c^--side of the crystal and the applied voltage, U, over the crystal was 2.0 kV in figure 5.3.b to 5.3.f.

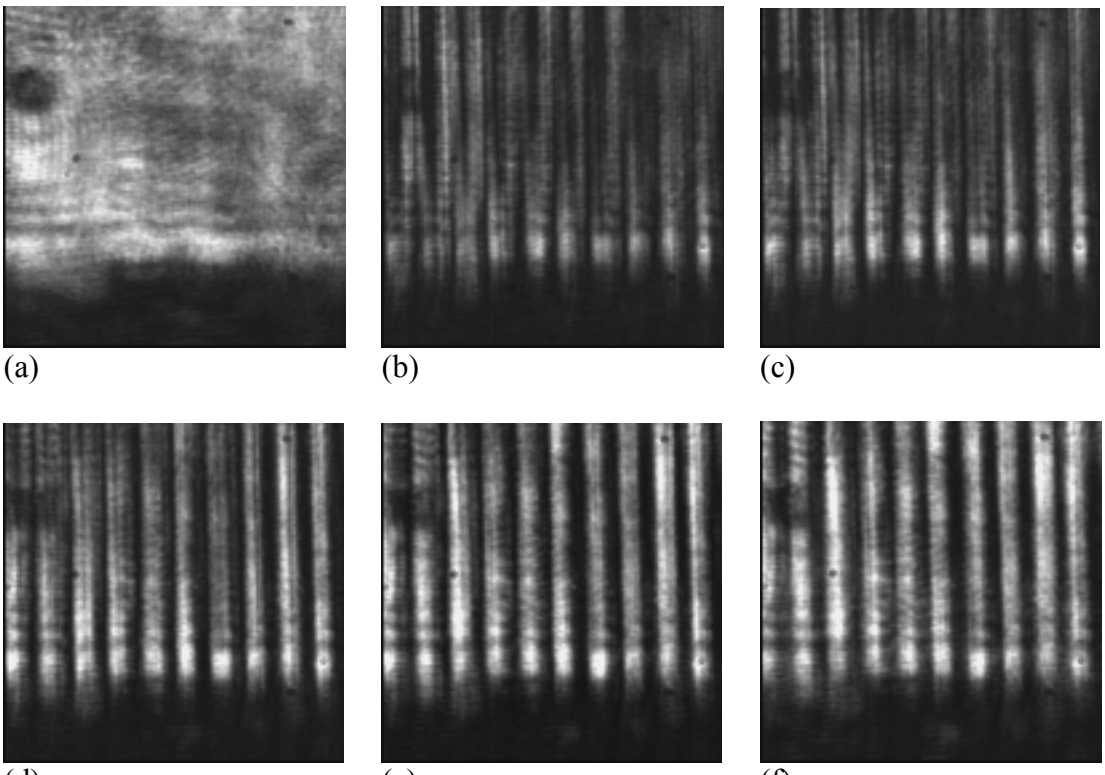

Fig. 5.3 Pictures from a poling sequence. U = 2.0 kV for picture b through f. (a): The picture was taken just before τ_{p1}, V = 0. (b): Picture taken at τ_{p1} + 1.1 ms, V = 0.27. The sample has started to pole. (c): The picture was taken at τ_{p1} + 2.2 ms, V = 0.37. (d): Picture taken at τ_{p1} + 4.4 ms, V = 0.55. (e): Picture taken at τ_{p1} + 6.6 ms, V = 0.61. (f): Picture taken at τ_{p1} + 8.8 ms, V = 0.55. Picture size 350 by 350 μm^2. Sample thickness 1 mm.

As illustrated by the picture sequence the periodic structure grew rapidly clearer with time and was very pronounced from τ_{p1} + 3.3 ms to τ_{p2}, with the contrast, V > 0.5. Simultaneously, the oscilloscope traces also confirmed poling with the other monitoring method. After τ_{p2}, the pattern vanished completely within 20 ms.

However, in other samples a weaker pattern could still be seen for a limited amount of time after the high-voltage pulse had been switched off. It was also observed in some samples, when so-called test pulses at U ≤ 1.5 kV were applied. The weak pattern could then be seen both during and after the voltage pulse, although no poling pulse had preceded these test pulses. The test pulses were used to extract additional information about the conductivity of the sample prior to the poling pulse was applied. Figure 5.4 shows the dependence of the visibility versus time after τ_{p2} for another sample, where several pulses at different voltages were used.

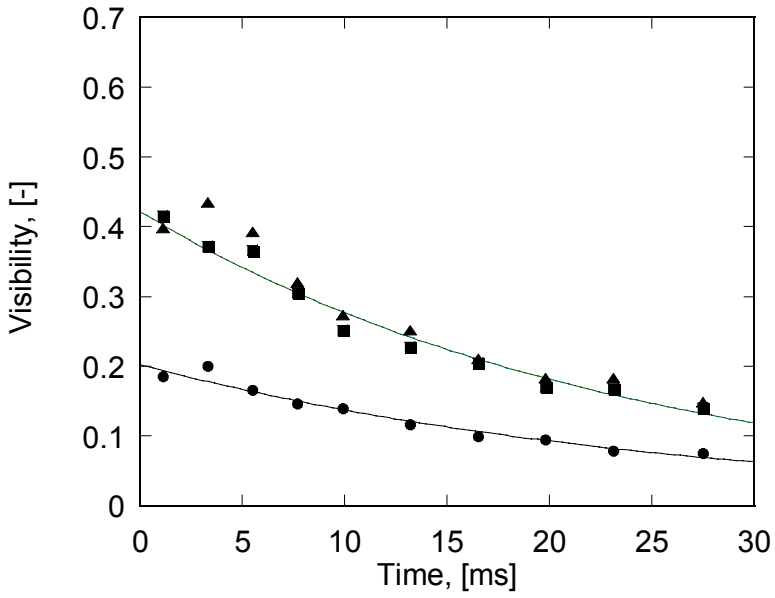

Fig. 5.4 The visibility of the pictures versus time after τ_{p2}. The three sequences where taken in a row. Sequence 1 = dots, U = 0.55 kV applied before τ_{p2}. Sequence 2 = triangles, U = 1.3 kV applied before τ_{p2}. Sequence 3 = squares, U = 2.0 kV applied before τ_{p2}. Sample thickness 1 mm. The two solid lines indicate exponential fits with time constant, $\tau \approx 26$ ms.

The proposed explanation for this phenomenon [IV] is that external charge carriers are injected periodically into the sample via the metallic finger electrode by the external voltage. These charges are trapped in defects of the lattice and they build up a periodic space-charge field, which modifies the external field periodically. When the

external voltage is switched off, the space-charge field decays due to internal ionic conduction and/or the finite lifetime of the charge carriers trapped in the defect levels. The decay is exponential with a time constant, τ, which in turn can be written as:

$$\tau = \frac{\tau_d \tau_c}{\tau_d + \tau_c} \qquad 5.3$$

where τ_d is the dielectric relaxation time constant and τ_c is the effective time constant for the other decay processes. The time constant $\tau \approx 26$ ms was measured for the sample in figure 5.4, and τ_d was calculated to $\tau_d = \varepsilon_0\varepsilon_r/\sigma \approx 16$ ms. τ_d should be the dominant time constant and the calculated and measured values agree fairly well. However the uncertainty of ε_r might be large, since it could only be estimated from ref. [52]. In other samples it was found that the space-charge field could relax faster than 1 ms.

After poling, the sample is probed to reveal evidence of the achieved grating. $U \leq 1.5$ kV for these probe pulses, in order to inhibit domain broadening. The sample mentioned above in figure 5.4 was poled during its third sequence. The pictures below were captured, in the three sequences that followed immediately after that poling pulse:

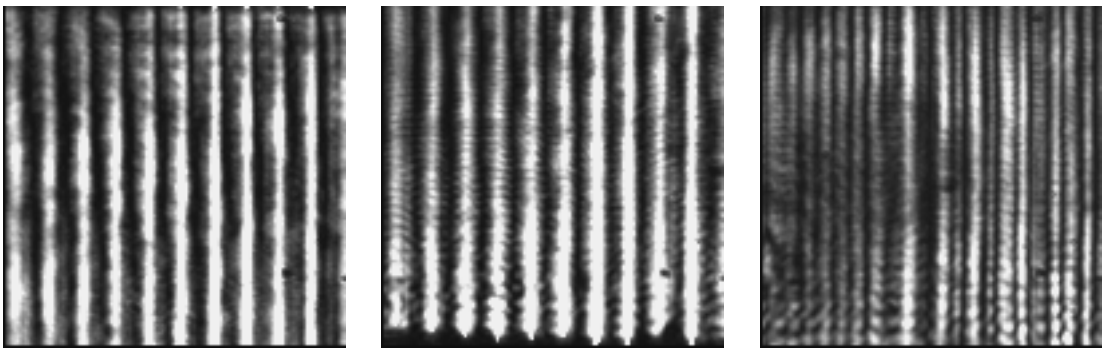

(a) (b) (c)

Fig. 5.5 Evaluation of the domain inverted structure. U = 1.4 kV, all pictures taken at τ_{p1} + 5.5 ms. (a) = sequence 4: Picture taken close to the original c^+-side, V = 0.68. (b) = sequence 5: Picture taken close to the original c^--side, right beneath figure 5.5.a, V = 0.71. (c) = sequence 6: Picture taken close to the original c^--side, approximately 5 mm to the side of figure5.4.b.

U = 1.4 kV for all sequences in figure 5.5 and all pictures within each sequence were very similar. Figure 5.5.a exhibits a very clear structure, containing ten full periods, as evidence for a successful poling of this part of the crystal. From the position close to the original c^+-side the camera was moved straight down to the original c^--surface. Figure 5.5.b illustrates that the periods have grown straight through the sample. The CCD camera was moved around in the x-z plane and it was discovered that the quality of the QPM grating varied along the x-axis. This is shown in figure 5.5.c, where the camera has been positioned 5 mm to the side of picture 5.5.b. Hence, with this non-invasive monitoring method it is possible to directly receive knowledge of the quality of the QPM grating.

5.6 High-order second harmonic generation for evaluation of the QPM grating

Evaluation of the quality of the periodic domain structure was also carried out through high-order SHG measurements. The conversion efficiency and the acceptance bandwidth were measured for the samples using a continuous wave Ti:Sapphire laser. From the acceptance bandwidth it is possible to calculate the effective gain length of the grating, i.e. the equivalent distance over which the grating can be considered to be perfect. This equivalent distance might be shorter than the length of periodic electrode due to missing reversals or other flaws in the grating that originated from the manufacturing process. However, usually I have assumed that the gain length is equal to the length of the periodic electrode and instead adjusted the nonlinear coefficient to receive agreement between the measured conversion efficiency and the calculated one. The fifth through tenth orders of SHG have been possible to reach for the OPO gratings in this thesis by scanning the wavelength of the Ti:Sapphire laser. The combination of a low order of SHG and simultaneously an output wavelength of the tuneable laser that can produce a high pump power have been preferable in order to achieve the highest possible conversion efficiency to reduce measurement uncertainties. Even orders of SHG have also been observed due to small deviations from the perfect 50% duty-cycle [II], [III]. As an example, a duty cycle of 54/46 will cause the sixth order second harmonic power to reach 50% of its peak value. The distribution of the sixth order frequency doubled power across the aperture of the PPKTP OPO crystal used in paper [II] and [VII] is shown in figure 5.6.

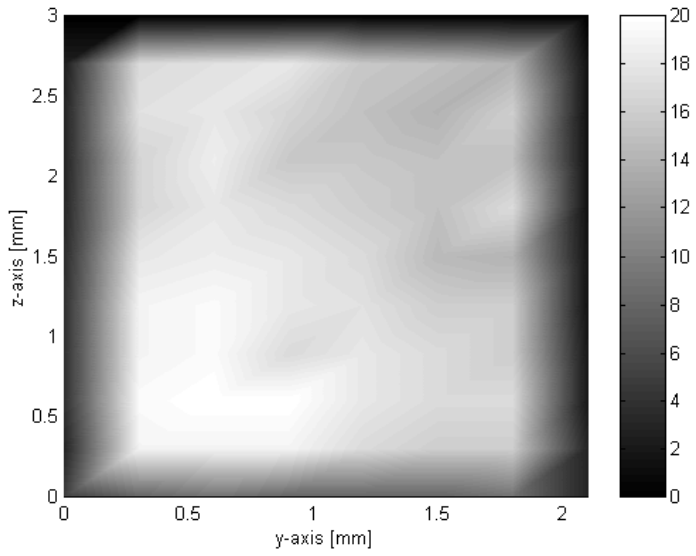

Fig. 5.6 Second harmonic power distribution across PPKTP aperture. 6^{th} order SHG.

The poled volume was 8 x 2 x 3 mm^3 (x,y,z). The pump beam ($w_0 \approx 50$ μm) was scanned over the aperture by moving the crystal through the beam. The grey-scale bar gives the second harmonic power in arbitrary units. Altogether 80 measurement points produced the map in figure 5.6. The standard deviation of the distribution is approximately 10% of its mean value, when data points that have been influenced by the clipping of the fundamental beam were disregarded. The effective nonlinear coefficient calculated from this measurement was $d_{eff} = 2d_{33}/\pi \approx 7.4$ pm/V. In good

agreement with the value of $d_{eff} \approx 8$ pm/V found from threshold measurements of the OPOs in the articles [II] and [VII], where this crystal was used as the nonlinear material.

6 Nanosecond optical parametric oscillators and amplifiers based on periodically poled $KTiOPO_4$

6.1 Introduction

Maiman made the first demonstration of the laser in 1960 [2] and at the very same moment he opened up for several new fields of research. One of them is the field of non-linear optics that was "born" already the year after, when Franken *et al.,*[85] could report on the first frequency doubling of light from a Ruby laser. Inspired by that work researcher started to investigate the possibilities of parametric down conversion. In 1965, Giordmaine and Miller[86], demonstrated the first optical parametric oscillator in a 5 mm long $LiNbO_3$ crystal. Since then extensive development of OPOs have been performed, which lead to rapid progress in the 1960's and 1970's. Harris[87] and Byer[5,6] made early reviews over the field of OPOs 1969 and 1979 respectively. The pace was then somewhat slower until the early 1990's, when the concept of electric field poling was demonstrated. The first periodically poled OPO in bulk material was fabricated from $LiNbO_3$ and was reported in 1995, [88], after that it has once again been a remarkable progress in the field of OPOs. Today, periodic poling of $LiNbO_3$ has turned into a mature industrial technology[30,75]. The first periodically poled KTP (PPKTP) OPO was operating in the femtosecond regime and was reported in 1997, [89]. The next PPKTP OPO was a doubly resonant continuous wave (cw) OPO demonstrated 1998 [90]. The first nanosecond PPKTP OPO journal article was published the year after, paper [I]. The earliest papers on periodically poled RTA (PPRTA)[91] and periodically poled KTA (PPKTA)[92] OPOs are from 1997 and 1999, respectively. Today, the technology for electric field poling of KTP and isomorphic compounds is being commercialised. At least two companies are manufacturing periodically poled KTP and its isomorphs, Cobolt AB, Sweden and Raicol Crystals Inc., Israel.

6.2 $KTiOPO_4$ versus other nonlinear materials

Flux grown KTP has been periodically poled and used as nonlinear material in this work because of KTP's many attractive properties. Another reason is of course that very little research had been done on parametric down conversion in PPKTP before this thesis started. As mentioned earlier the material posses a high nonlinear coefficient d_{33} = 16.9 pm/V, the material is transparent to approximately 4.3 μm, it has high optical damage threshold, it is insensitive to photorefractive effects and has low susceptibility for grey-tracking. An important feature is also that the coercive field of KTP is only ~2 kV/mm, which gives the opportunity to pole thicker samples. OPO's in a 3 mm thick PPKTP crystal are demonstrated here, [II], [VII]. The non-poled material is also available from several vendors to a reasonable price.

As seen in tables 4.3 and 4.4 the nonlinear properties between the isomorphic compounds are very similar and they could also be candidates as nonlinear material. However, the high conductivity of KTA has limited the sample thickness of periodically poled KTA (PPKTA) to 0.5 mm so far and the crystal growers have from

time to time had major difficulties in deliver both RTA and RTP of high enough quality to be suitable for periodic poling.

Congruent $LiNbO_3$ (CLN) is by far the most extensively used material for QPM so far. CLN is attractive for periodic poling, since it is a very mature nonlinear material. It is available in wafers up to 4 inches in diameter with good homogeneity and good optical quality. Today, periodically poled CLN (PPCLN) samples > 50 mm are routinely poled[75]. The optical properties are favourable with d_{33} = 27.2 pm/V and a transparency from approximately 0.35 to 5.4 μm. A considerable disadvantage though is its high coercive field of ~21 kV/mm [30], which has limited the PPCLN crystals to a thickness of ~1 mm. There have been tries to circumvent the problem e.g. through bonding of several thinner crystals to form a 3 mm thick PPCLN sample[93]. However, it is complicated to achieve good alignment of the individual pieces and the damage threshold is lowered, due to total internal reflections between the crystal interfaces. Congruent $LiTaO_3$ (CLT) is transparent down to ~0.28 μm but have otherwise similar properties to CLN. A drawback is that the photorefractive effect plagues both PPCLN and PPCLT and because of that they have to be operated at elevated temperatures to avoid damage or substantial reduction of the device efficiencies. They have also lower optical damage thresholds than for example KTP. One way to reduce the risk of inducing the photorefrative effect in $LiNbO_3$ and $LiTaO_3$ is to dope the material with Magnesium Oxide (MgO) to increase the conductivity. For example a 1 mm thick, high average power nanosecond MgO:PPLN OPO operating at room-temperature has been constructed[94]. The quality and homogeneity of these doped wafers though seem to vary to a large extent, and they have not yet reached the same high quality that is available for the undoped ones. Researchers have recently been able to grow stoichiometric $LiTaO_3$ (SLT) with a quality suitable for periodic poling. SLT is attractive since it has a coercive field one order of magnitude lower than CLT, ~2 kV/mm, which could lead to poling of thicker samples. A 3 mm thick nanosecond PPSLT OPO was demonstrated recently[95]. However, the pump beam radius was only 0.5 mm. Once again are the homogeneity and quality of the material issues that are not solved satisfactorily yet.

Still another material to consider is Potassium Niobate, KN, which has been periodically poled by Meyn *et al*.[34]. The nonlinear coefficient is similar to KTP's, d_{33} = 19.5 pm/V and no photorefractive effect was observed in that study. Up until now has only one OPO based on PPKN been reported[96].

Beta-Barium Borate, β-BaB_2O_4 (BBO) and Lithium Triborate, LiB_3O_5 (LBO) are also crystals that have been extensively used in nonlinear optical processes[97]. They posses a very high optical damage threshold >10 GW/cm^2 when pumped at 1.064 μm with a few nanosecond long pulses and they have low optical losses, but their nonlinear tensor elements have only a magnitude on the order of approximately 1 pm/V [68]. Furthermore, these two materials are not ferroelectric[a], and thus not possible to pole. For that reason they will not be discussed further in this thesis.

As a summary of this section it can be said that different materials will be the best choice as nonlinear medium for different applications and situations. PPKTP is a very

[a] This is to my knowledge the prevailing opinion among researchers today and the materials have not been periodically poled so far.

attractive and competitive nonlinear crystal, especially for nanosecond parametric down conversion when high peak intensities are needed. The fabrication and characterisation of the PPKTP material, as well as the design, development and characterisation of nanosecond PPKTP OPO's and OPA's have been investigated in detail in this work.

6.3 General experimental conditions

In the experiments of the optical parametric oscillators and amplifiers that have been performed in this thesis certain experimental conditions have been more or less the same. If not explicitly stated otherwise the following conditions apply: As previously stated in this thesis, flux grown KTP has been periodically poled and used as nonlinear medium. The grating vector of the QPM structure has been parallel to the principal x-axis of the crystal and all interacting fields were polarised along the z-axis. Most OPOs and OPAs were pumped at 1.064 μm with nanosecond pulses (5 – 12 ns), (except in paper [VIII] and [IX]). The operation of the devices has mostly been at room-temperature. The beam quality parameter M^2 and the beam waists were measured manually by the "scanning knife-edge method"[98,99] in our laboratory. Fast photodetectors and an oscilloscope were used for the measurements in the time domain. The duration of the pulses is stated as full width at half maximum values (FWHM) and beam waists are given at the radius where the intensity has been reduced to $I = I_0 e^{-2}$. Please, refer to the appendix [I] - [IX] for further details.

6.4 Parametric gain and amplification

In the case of parametric amplification there are two fields incident to the crystal, see figure 2.2. The strong pump field at frequency ω_p and a weak signal field at ω_s. These fields mix together through the nonlinear response of the crystal and produce a polarisation at a third frequency ω_i. Provided that the process is phasematched this new field will grow with distance. This idler field then mixes again with the pump and produces a polarisation at the signal frequency. The energy and momentum conservation conditions for the processes are:

$$\begin{aligned} \omega_p &= \omega_s + \omega_i \\ \Delta \boldsymbol{k}_{tot} &= \boldsymbol{k}_p - \boldsymbol{k}_s - \boldsymbol{k}_i - \frac{2\pi m}{\Lambda}\boldsymbol{e}_x \end{aligned} \qquad 6.1$$

As discussed in chapter 3, QPM is applicable for all second order nonlinear mixing processes. The phasematching condition for an effective process to take place becomes $\Delta\mathbf{k}_{tot} \approx 0$. Note, that this is a vector equation where $\mathbf{e}_x$ is the unit vector parallel to the grating normal.

On the photon level this means that each pump photon is split into two new photons, the signal and the idler photon, and both fields grow with distance. The division of the pump photon into two parts is manifested in the so-called Manley-Rowe relation, which can be deduced directly from equation 2.8 [3].

$$-\frac{W_p}{\omega_p}=\frac{W_s}{\omega_s}=\frac{W_i}{\omega_i} \qquad 6.2$$

The relation holds provided that there are no losses in the material. Here, W_j j = p, s, i stands for the power input to unit volume of the medium from the pump, signal and idler, respectively.

If it is reasonable to assume that the pump beam is not depleted in the amplification process and that the fields do not experience any losses, the equation system 2.8 can be solved and yield the following result for the growth of the signal field:

$$\frac{I_s(L)}{I_s(0)}=1+G=1+(gL)^2\frac{\sinh^2\left(\sqrt{(gL)^2-\left(\Delta k_{tot}L/2\right)^2}\right)}{(gL)^2-\left(\Delta k_{tot}L/2\right)^2} \qquad 6.3$$

$$g^2=\frac{2\omega_s\omega_i d_{eff}^2 I_p}{\varepsilon_0 c^3 n_p n_s n_i}$$

g is the gain coefficient. In the case of only small signal gain i.e. $\Delta k_{tot}/2 >> g$, the gain G will have the familiar $sinc^2$ dependence as in equation 2.11 and grow with distance squared and with the incident pump intensity.

$$G=(gL)^2 sinc^2\left(\frac{\Delta k_{tot}L}{2}\right) \qquad 6.4$$

In the case of very strong gain, $g >> \Delta k_{tot}/2$, the signal and idler field will experience exponential gain and the result will be:

$$\begin{aligned} I_s(L)&=I_s(0)\cosh^2(gL)\\ I_i(L)&=I_i(0)\sinh^2(gL)\end{aligned} \qquad 6.5$$

The need for a weak signal field at the input side may become unnecessary if the gain is strong enough, since the generated fields can grow directly from noise. This is called optical parametric generation, OPG.

KTP's high resistance against optical damage and high nonlinear coefficient makes the material suitable as gain medium in optical parametric amplifiers, OPAs. Although PPKTP samples are typically 20 mm long compared to crystals of PPLN, which might be up to 50 mm, the possibility to pump PPKTP at higher intensities can compensate for shorter gain length. In paper [III], we demonstrate this in a PPKTP sample of only 12 mm length. The OPA was pumped by a flash-lamp pumped Nd:YAG laser at 1.064 μm. The duration of the pulse was 5 ns and repetition rate 20 Hz. The pump beam was mixed with a continuous signal beam of 6 mW at 1.54 μm from an Er-Yb:glass microchip laser[100] and the signal amplification resulted in 3 ns pulses with peak power of ~24 kW i.e. the signal gain reached 66 dB. The peak

intensity of the pump beam was then ~925 MW/cm^2, assuming a Gaussian spatial beam profile, ($M^2 \approx 2.6$, measured). The dependence of the output signal pulse energy on pump pulse energy for the OPA is plotted in figure 6.1.

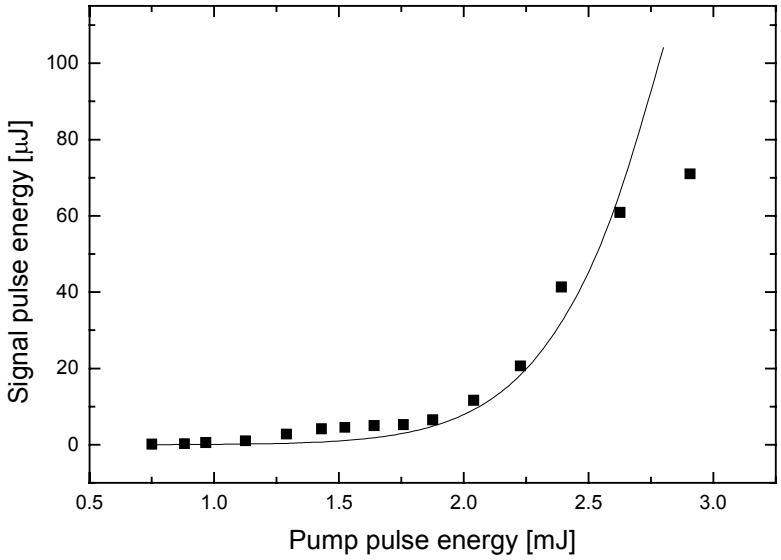

Fig. 6.1 Signal energy in dependence of pump energy for the OPA in paper [III]. The seed pulse energy is equivalent to 18 pJ.

The software packet "SNLO" provided the theoretical fit to the experimental data[101]. The program solves the coupled wave equations for the interacting fields numerically in two spatial dimensions and the time domain simultaneously. Since a substantial amount of the idler was absorbed at 3.4 μm, a 51% cm^{-1} power loss was assumed from figure 4.3 [71]. The nonlinear coefficient was used as fit parameter and the best fit gave $d_{eff} \approx 9.7$ pm/V, which corresponds to $d_{33} \approx 15.2$ pm/V. This is the highest reported value so far for a PPKTP parametric device and it is a proof of the high quality of the QPM structure. The offset of the right most point in figure 6.1 is probably due to minor grey-track formation, which caused an increase in the absorption of the material. However, the grey-track formation was then reversible. Doubling the beam waist and the gain length should not impose any problems, but would allow the energy of the output pulses from the device to approach the milijoule level.

An OPA presents an interesting route to control of the output spectrum. Narrow bandwidths of the signal can be preserved provided that the pump bandwidth is narrow. In paper [V], an input signal bandwidth < 400 MHz was unchanged by the amplification process. The amplification though was rather modest for this case. This topic will be further discussed in the paragraph regarding bandwidths.

6.5 Nanosecond optical parametric oscillators

Mirrors can be used to provide positive feedback of the generated fields, to enhance the efficiency of the parametric process and to avoid pump intensities close to the damage threshold. If one field is resonated the OPO is called singly-resonant (SRO) for a doubly resonant OPO (DRO) are both the generated fields resonated. It is also an

option to have the pump reflected back into the cavity in a double pass configuration. The letters DP are then added to the abbreviation, e.g. DPDRO, see figure 6.2.

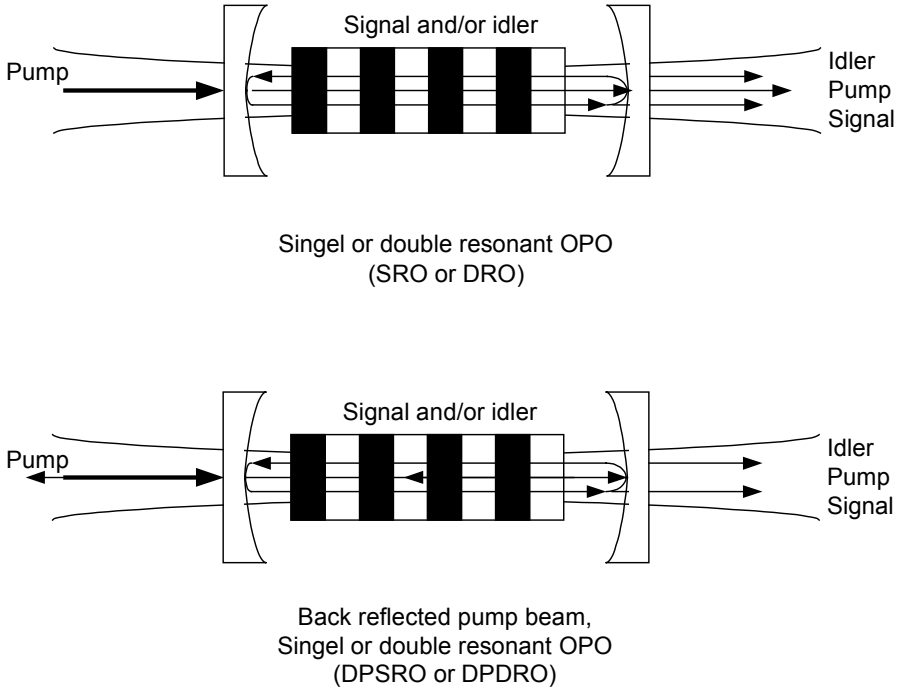

Fig. 6.2 Examples of cavity configurations for optical parametric oscillators

SRO, DRO and DPDRO cavities have been investigated in this work. Another type of cavities apart from these linear ones in figure 6.2, is of course ring cavities.

An OPO is in some ways very similar to a laser[102]. The parametric gain from the nonlinear process must exceed the total losses of the cavity for any field to build up inside the resonator and for the OPO to be able to deliver the signal and idler waves. Once this threshold has been passed the OPO will efficiently convert the pump beam to tuneable signal and idler waves. A second condition for the OPO to function appropriately is that the signal and idler frequencies must correspond to two longitudinal modes of the cavity. This will cause stability problems in DROs if not special steps are taken[103]. Analogous to the laser an OPO can also operate on one or several longitudinal modes, depending on the design criteria of the cavity and on the quality of the pump laser. The biggest advantage with DROs is that the threshold is lowered compared to SROs. However, the nonlinear crystal can not store broad band incoherent spectral energy the same way a laser crystal can, the nonlinear medium just provides a nonlinear reactance to the different fields involved in the frequency mixing, and phase coherence between the fields is very important for an OPO.

In the formulas of paragraph 6.4 above it was assumed that the interacting fields were plane waves, but to reach sufficient gain for parametric down conversion, it is often necessary to focus the pump beam, which has a more or less Gaussian spatial profile. Boyd and Kleinman[9] have also studied different focussing conditions for Gaussian beams in the case of parametric processes. They came to the conclusion that the most efficient conversion will occur, if all waves have a common confocal parameter, b, defined as:

$$b_j = \frac{2\pi n_j w_{0j}^2}{\lambda_{0j}} \qquad 6.6$$

j = p, s or i, i.e. $b_p = b_s = b_i = b_0$. Physically, the confocal parameter is equal to the distance around focus where the beam radius is smaller than $\sqrt{2}w_0$, i.e. two Rayleigh lengths[102]. The confocal parameter is reduced with a factor 1/ (M^2) for a beam with $M^2 > 1$, [99]. The M^2 factor is defined as $M^2 = \Theta/\theta$, where Θ is the multi-mode beam divergence and θ is the divergence for a perfect Gaussian beam with the same waist[99]. The gain coefficient will be modified as follows, if absorption is neglected and the focus is in the middle of the crystal:

$$g^2 = \frac{4\omega_s \omega_i d_{eff}^2 P_p}{\varepsilon_0 c^3 n_s n_i \lambda_p L} \bar{h}_m(B,\xi) \qquad 6.7$$
$$\xi = L \big/ b_0$$

The double refraction parameter, B, is defined as: $B = \rho(Lk_0)^{1/2}(n_p/n_o)^{1/2}/2$, but all the fields in this work have been polarised parallel to the z-axis, and hence B = 0, since ρ = 0 for our cases. The function $\bar{h}_m = (B,\xi)$ versus ξ and B is shown in figure 6.3:

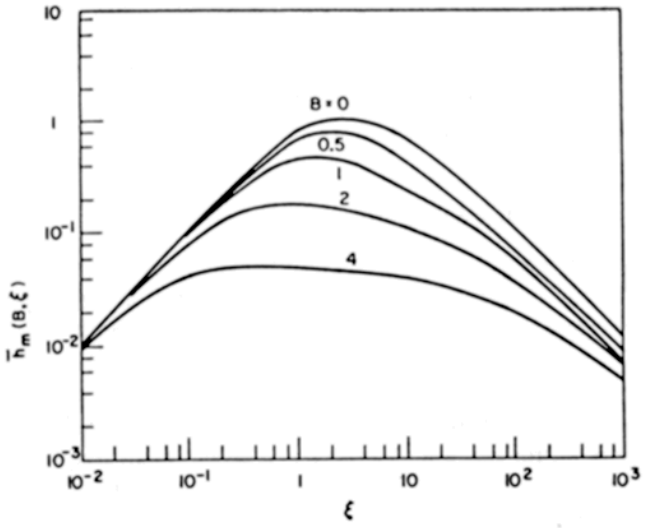

Fig. 6.3 Parametric gain reduction factor for focused Gaussian beams[9,13].

As illustrated in the graph, the gain is at maximum if no double refraction is present. The curve is actually identical for SHG and parametric gain when B = 0. The maximum $\bar{h}_m(0,\xi) = 1.068$ occurs for ξ = 2.84. In the case of weak focussing is $\xi < 1$ and the asymptotic behaviour is given by:

$$\bar{h}_m(B,\xi) \longrightarrow \xi \quad \left(\xi < 0.4; \xi < 1/6B^2\right) \tag{6.8}$$

If this result is substituted into equation 6.7, the gain coefficient in equation 6.3 will be recovered. For all the resonators presented in this work with two plane mirrors the pump beam spot sizes at focus have been large enough for the plane wave approximation to be valid, although $M^2 \neq 1$.

6.6 Thresholds for nanosecond OPOs

The threshold for an OPO is reached when the parametric gain equals the total losses of the cavity. Brosnan and Byer[73] have developed a theory to calculate the threshold intensity analytically for nanosecond SROs. The formula was slightly modified by Marshall *et al*., in order to use the time τ measured at FWHM of the pulse[104]. The threshold intensity is then given as:

$$I_{th} = \frac{1.8}{\kappa g_s L_{eff}^2 (1+\gamma)^2}\left(\frac{25 L_{cav}}{c\tau} + 2\alpha_p L + \ln\frac{1}{\sqrt{R}} + \ln 2\right)^2 \tag{6.9}$$

where $\kappa = g^2/I_p$, L_{eff} is the effective gain length, L_{cav} is the optical length of the cavity, γ is the ratio of the backward to forward pump amplitude in the cavity and $R = R_{in}R_{out}(1-R_c)^4$. R_{in}, R_{out} and R_c are the incoupling, outcoupling and end-face reflectivities respectively. g_s is the mode-coupling coefficient of the pump and signal beams. Note that α_p is the power absorption coefficient.

$$g_s = \frac{w_{0p}^2}{w_{0p}^2 + w_{0s}^2} \tag{6.10}$$

In paper [I], we studied four different OPO cavities with two different PPKTP crystals and calculated the effective nonlinear coefficient from the measured OPO thresholds using equation 6.9. The sample lengths were 20 mm for crystal A and 15 mm for crystal B.

	Reflectivities [%]			Measured Threshold		
Sample	R_{in}	R_{out}	R_c	E_{th} [mJ]	I_{th} [MW/cm$_2$]	d_{eff} [pm/V]
A	90	90	4	0.24	27	6.1
A	90	50	4	0.33	36	6.4
B	40	40	9	0.50	66	8.7
B^{DRO}	9	9	0	1.25	164	5.3

Table 6.1 Effective nonlinear coefficient deduced from measurements of the OPO thresholds.

The last OPO in table 6.1 was considered to be doubly resonant, since it was oscillating on the uncoated end-faces of the crystal only. To calculate the threshold for

this DRO we used a modified version of equation 6.9, see ref. [105]. The deviation between the two values of d_{eff} for sample B is attributed to the lack of external cavity mirrors for the DRO. The end-faces of sample B were not perfectly parallel, and this increased the threshold significantly, when the external mirrors were taken away from the cavity and hence the value of the effective nonlinear coefficient was lowered.

Equation 6.9 was also used to determine the d_{eff} from the threshold measurements of the 3 mm thick SRO in paper [II]. Six different cavity lengths were used to decrease measurement uncertainties. The SRO had a $d_{eff} \approx 8.0$ pm/V, which is within 8 % from the value of 7.4 pm/V measured by sixth-order SHG.

The lowest pulse energy threshold for a SRO presented in this thesis was 50 μJ, paper [VII]. The pulse length was 6 ns and the repetition rate 10 kHz, the signal was mode-matched with the pump beam ($M^2 \approx 1.2$) and the output coupler had a signal transmission of 7 %. This should be compared with the low threshold PPLN SRO presented in ref. [106] with a 6 μJ threshold. This PPLN sample though was 26 mm long, 2.6 times longer than the 10 mm PPKTP crystal used above. The pump and cavity parameters were otherwise comparable, besides that the PPLN sample was uncoated.

The lowest DRO threshold was found to be 10 μJ for the 532 nm pumped OPO in paper [IX].

6.7 Conversion efficiency

Optical parametric oscillators have the potential of being very efficient frequency converters. First the case of continuous wave (cw) OPOs is discussed. Once the cw OPO has reached threshold under steady-state conditions, the gain will be clamped at the threshold level and every additional pump photon will be converted to signal and idler output photons. Bjorkholm has calculated theoretical conversion efficiencies for pump beams with Gaussian spatial profile[107], both for SROs and DROs. He came to the conclusion that 100 % conversion efficiency can not be reached using Gaussian beams. In the case of SRO the highest efficiency of 71 % is achieved at ~6.5 times the threshold. The explanation is that the wings of the Gaussian beam are generally below threshold and they are not converted. In the case of a DPDRO close to degeneracy Breitenbach *et al.*[103] theoretically found that 100 % conversion efficiency is possible during certain circumstances also for focussed beams. In the same article they experimentally demonstrated a total efficiency of 81 % for a cw OPO in MgO:PPLN. For pulsed OPOs there will be a finite build up time for the fields before steady state conditions in the cavity is reached and because of that the energy conversion efficiency is lower than the peak power efficiency. The reduction factor is approximately the ratio of the signal to pump pulse widths, which can be written as 1-1/N, where N is the number of times above threshold[108]. The energy conversion efficiency, η, is defined as:

$$\eta = \frac{E_s + E_i}{E_p(0)} \qquad 6.11$$

E_j , j = p, s or i is the pulse energy of the pump, signal or idler respectively and has been used here.

The dependence of output energy versus pump energy will be linear as shown theoretically and experimentally by Terry *et al.*,[108] as long as no substantial back-conversion from the generated waves to the pump wave is occurring. This linear behaviour is seen in many of the OPOs presented here. Weak tendencies of decreasing conversion efficiency at high intensities and hence a deviation from the linear dependence due to back-conversion can be seen in figure 2 of paper [II].

Depletion of the pump pulses in the time domain was studied in paper [I]. Back-conversion was observed for the very highest pump intensities. The temporal profiles though were not spatially integrated over the entire beam area and the photodiode detected only a smaller part of the beam around the beam axis. This explains why the output energy is still almost linearly proportional to the pump energy at high intensities, although back-conversion takes place at the centre of the beam. Smith *et al.*, have investigated pump-deletion and back-conversion in detail[109].

Please note that in the first article (paper [I]) we assumed that an equal amount of energy was flowing in both directions out of the cavity for the case of crystal B and the mirrors with 40 % signal reflectivity. However, after having gained deeper insight in how optical parametric oscillators perform we have realised that this assumption has some deficiency. The assumption was justified by the measurement of the depletion of the pump, which was consistent with 50 % conversion efficiency. I would like the reader to only consider the energy flowing in the direction of the pump from this cavity (0.9 mJ). There were energy flowing in the backward direction but we made no measurements of its magnitude. In the case of crystal A and two mirrors with 90 % reflectivity the assumption of equal amounts of energy in both directions is better. This was also verified in paper [II], where 52 % of total conversion efficiency (4.5 mJ in the forward direction and 3.8 mJ in the backward direction) was measured with the same mirror reflectivities.

In the following text I will only consider total energy efficiencies, i.e. both signal and idler, measured in the direction of the pump. The highest conversion efficiency we have measured in this work is just above 50 % for the degenerate DRO pumped at 0.532 μm in paper [IX]. The highest SRO efficiency is 45 % for the large aperture PPKTP crystal [II].

6.8 Generated pulse energies and average powers

One of the greatest advantages with KTP is that the low coercive field allows thicker samples to be poled. After the initial experiments on PPKTP OPOs in paper [I], it was natural to try to scale the output pulse energies. The highest total output pulse energies (signal + idler) reached 18.3 mJ (η = 35 %) for the SRO in paper [VII]. It was pumped by a Nd:YAG laser at 1.064 μm, 10 Hz and $\tau \approx 11$ ns. The beam waist radius was 1.15 mm to fill out the aperture properly. The output energy could be compared to the 11 mJ that was achieved from the PPCLN OPO reported in ref. [93], although the pump beam in that case had to be elliptical to fit in the 1 mm thick sample.

It is necessary to have a sample that is homogeneously poled with high quality over the entire volume of the crystal to reach high output pulse energies. The quality of the QPM grating for the 3 mm thick PPKTP sample mentioned above was evaluated in a SRO pumped by a high repetition rate laser (10 kHz) [VII]. Figure 6.4 shows a map of the output power over the aperture of the sample. The pump beam radius was 130 μm and it was probing the sample in 50 x 42 points. The output power was measured at a constant pump power. The map in figure 6.4 gives a direct image of the quality of the QPM structure.

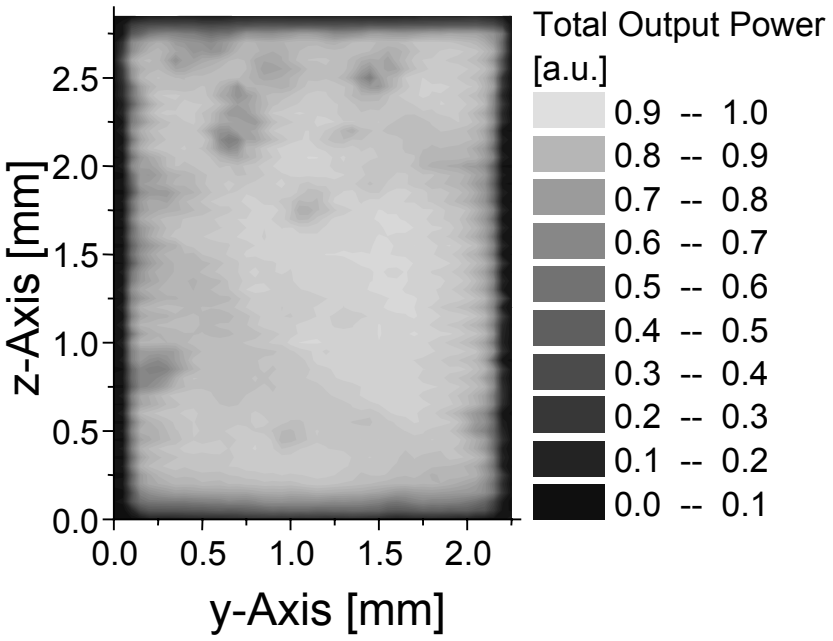

Fig. 6.4 Total PPKTP SRO output power as function of the crystal position in the y-z-plane.

The standard deviation of the output power in figure 6.4 is only 8% of the mean value. Figure 6.4 should be compared with figure 5.6, which shows the same crystal aperture. As seen, both pictures show the same excellent quality of the QPM grating.

To raise the average output power, the pump laser was set to run at 20 kHz and it then produced 7.2 W, at maximum. The generated signal + idler power at that point was 2 W (η = 28 %), this is the highest average output power from a PPKTP OPO reported so far [VII].

However, we have measured, in up to this point unpublished experiment, average output powers reaching 24 W from a PPKTP DPDRO. The experiments were made in collaboration with Dr. Y. Hirano at Mitsubishi Electric Corporation in Japan. The pump laser was a high brightness diode pumped Nd:YAG laser, producing 40 ns pulses at 15 000 pulses per second (15 kpps), but the repetition frequency of the laser was 60 kHz, which means that the operating duty-cycle of the Q-switch is 25/75. The beam quality of the laser was very high, $M^2 \approx 1.1$. It was focussed into a spot of 250 μm radius in the 1 mm thick PPKTP sample of 20 mm length, Λ = 38.85 μm. The crystal was temperature controlled at 40 °C by a Peltier element, and the output wavelengths were then 2.01 μm and 2.26 μm. Degeneracy was reached at

approximately 70 °C. The cavity was 60 mm long. The input coupler was flat, antireflection coated for the pump and R ≈ 99 % for the signal and idler. The output coupler was slightly curved, radius of curvature 2 m, 100 % reflective for the pump and approximately 35 % reflective for the signal and idler. The sample was in these preliminary experiments left uncoated. Figure 6.5 shows the generated OPO output power in dependence of the pump power.

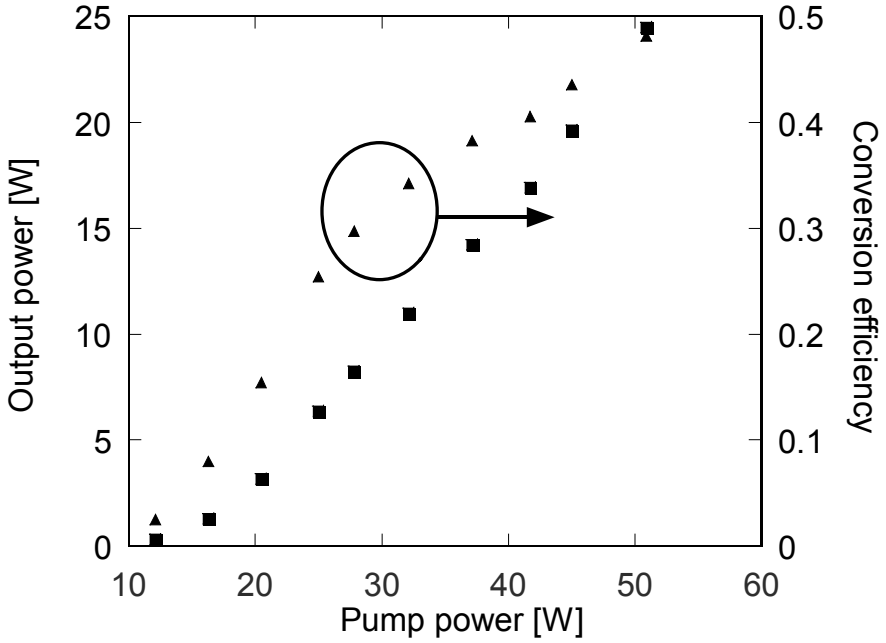

Fig. 6.5 High average power double pass doubly resonant OPO in PPKTP. Squares = output power. Triangles = conversion efficiency.

The total conversion efficiency reached 48 %. The maximum intensity was 181 MW/cm^2, which corresponds to 512 MW/cm^2 at 5 ns, where the intensity damage threshold is scaled as[110]:

$$I_{dam,5ns} = \sqrt{\frac{\tau_{40ns}}{\tau_{5ns}}} I_{dam,40ns} \tag{6.12}$$

After these initial experiments, the sample was sent for antireflection coating, when it returned the goal was to achieve even higher output powers. Unfortunately, the sample was destroyed during this second round of experiments. It burned from the exit surface of the crystal towards the centre along the pump beam path, when the peak intensity reached 128 MW/cm^2 (corresponding value at 5 ns is 413 MW/cm^2). The reason for the optical damage is not clear. We believe that it was a combination of circumstances. The pump beam might have been slightly miss-focussed, the crystal might have had a weaker spot at the focus and/or the coating might have reduced the damage threshold at the exit surface of the output wavelengths. Further investigations should be performed to explore the limit of PPKTP in terms of high power OPOs. It should be possible to further approach the excellent results of a MgO:PPLN DPDRO (57 W output power at 71 % conversion efficiency) reported by Hirano *et al*.[111]

6.9 Tuning of optical parametric oscillators

A very attractive feature of OPOs is that they are tuneable. The governing equations are:

$$\begin{aligned} &\omega_p = \omega_s + \omega_i \\ &\frac{n_p\omega_p}{c}\boldsymbol{e}_p = \frac{n_s\omega_s}{c}\boldsymbol{e}_s + \frac{n_i\omega_i}{c}\boldsymbol{e}_i + \frac{2\pi m}{\Lambda}\boldsymbol{e}_x \end{aligned} \qquad 6.13$$

Tuning is achieved for example by varying the refractive indices, the frequencies, the grating period and/or the cavity length. The direction of propagation of the beams is also important since the lower equation in 6.13 is a vector equation. The refractive index can be affected in many ways since it is in general a function of wavelength, temperature and propagation direction etc. Expanding the lower equation in the tuning variable ζ and the signal frequency gives the tuning rate:

$$\begin{aligned} &\frac{d\omega_s}{d\zeta} = \frac{1}{\beta}\left[\frac{\partial k_p}{\partial\zeta} - \frac{\partial k_s}{\partial\zeta} - \frac{\partial k_i}{\partial\zeta} - \frac{\partial K}{\partial\zeta}\right] \\ &\beta = \frac{\partial k_i}{\partial\omega_i} - \frac{\partial k_s}{\partial\omega_s} \end{aligned} \qquad 6.14$$

The most common method to tune QPM OPOs is to vary the temperature of the periodically poled sample. The dependence of the frequency tuning-rate on temperature, including the expansion of the grating, is given by:

$$d\omega_s = \frac{\left(\left[\omega_p\frac{\partial n_p}{\partial T} - \omega_s\frac{\partial n_s}{\partial T} - \omega_i\frac{\partial n_i}{\partial T}\right] + \alpha_x\left[n_p\omega_p - n_s\omega_s - n_i\omega_i\right]\right)dT}{\left(n_s - n_i + \omega_s\frac{\partial n_s}{\partial\omega_s} - \omega_i\frac{\partial n_i}{\partial\omega_i}\right)} \qquad 6.15$$

We have in paper [VII] reported on the temperature tuning behaviour of four different PPKTP OPOs. The experimental data points were fitted with the theory given by Ghosh[69].

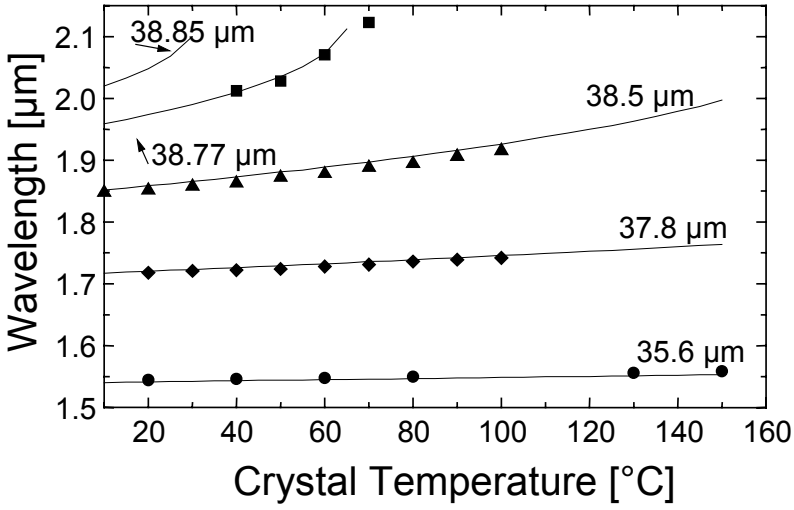

Fig. 6.6 Temperature tuning of four different PPKTP OPOs.

As seen in figure 6.6 the tuning-rate is rather slow far from degeneracy.

Another frequently utilised technique to tune QPM OPOs is to have several different grating periods next to each other in one crystal. A PPCLN OPO was tuned from 1.36 to 4.83 µm, a total of 3.47 µm by translating the sample containing 25 different gratings through the pump beam at 1.064 µm [37]. Gratings that are fan shaped have also been tried[38].

It is also a possibility to use non-collinear phasematching schemes to increase the tuning range. We report in paper [IX] on a non-collinear OPO pumped at 0.532 µm. The pump beam and the grating vector were parallel with the x-axis, but the cavity axis was rotated from the x-axis with an angle θ. Rotating the cavity by 5.6° from collinear propagation provided a tuning from 0.98 µm to 1.164 µm at room temperature. Combining the non-collinear phasematching with temperature tuning gave a total tuning range of 0.295 µm, from 0.94 µm to 1.235 µm. This particular scheme has the disadvantage that the cavity axis i.e. both mirrors have to be rotated around the sample. This could of course be made easy by some clever mechanics, but it would be even simpler to just rotate the sample itself. The interacting waves will also be affected by the lateral walk-off between the beams due to the geometry of the phasematching and this in turn will lower the efficiency of the OPO.

In paper [VI], we demonstrated for the first time a QPM OPO based on a crystal with cylindrical shape. The OPO had a fixed cavity axis and the pump and the signal beams were always parallel to this axis. The grating vector was turned an angle α from this cavity axis by just rotating the sample. The idler was free to fulfil the phasematching condition. The 0.5 mm thick PPKTP sample used had a period of 35 µm and was poled over an area of 10 x 10 mm^2. This type of non-collinear OPO has several advantages. First it provides truly continuous and very wide spectral tuning. A drawback with multigrating crystals are that the tuning is stepwise, the shift from one grating to the next will have to take some finite time. Fan-shaped gratings on the other hand provide continuous tuning but will impose a spectral heterogeneity to the output beams, since the grating period is varying over the beam area. The lateral walk-off in

the case of the "cylindrical OPO" due to the phasematching geometry is very small [VI] and because of that it is possible to have the same threshold and efficiency over the entire tuning range. The tuning range of the "cylindrical OPO" was from 1.515 μm (3.560 μm) to 2.040 μm (2.220 μm) for the signal (idler) in total 0.52 + 1.34 = 1.86 μm, when the sample was rotated 26°, see figure 6.7.

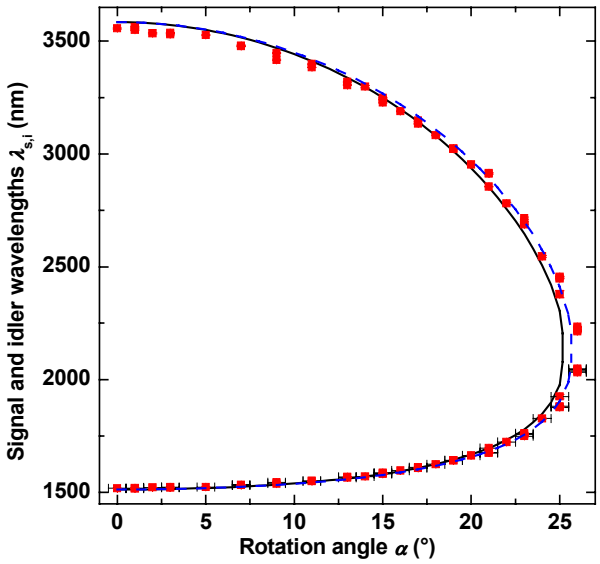

Fig. 6.7 Tuning of the OPO based on a cylindrical PPKTP sample.

This is the largest tuning range reported so far for a PPKTP OPO.

6.10 Bandwidth

The gain bandwidth and the total spectral bandwidth given by the cavity are other spectral properties that are important for OPOs. For example, it is desired in many spectroscopic applications to have a narrow spectral bandwidth of the generated light. The gain bandwidth is defined from the relation $\Delta kL/2 = \pi$. In order to calculate the gain bandwidth, the phase-mismatch between the interacting waves Δk is expanded as a function of frequency in a Taylor series and the result is set equal to $2\pi/L$. Δk may be used instead of Δk_{tot} in the calculation above, since the grating wave vector is independent of the frequency for a constant period[15]. In experiments is the bandwidth at FWHM more often determined. The factor between the two definitions is 0.886. The gain bandwidth (FWHM) for an optical parametric process at low gain and far from degeneracy is thus given as:

$$\Delta\omega_s = \frac{5.57c}{L\left|n_s - n_i + \omega_s \frac{\partial n_s}{\partial \omega_s} - \omega_i \frac{\partial n_i}{\partial \omega_i}\right|} \qquad 6.16$$

Close to degeneracy or close to a turning point in the dispersion curve it is necessary to retain terms of second order in the series expansion. Equation 6.16 is then modified to:

$$\Delta\omega_s = \frac{3.33\sqrt{c}}{\sqrt{L\left(4\frac{\partial n_s}{\partial \omega_s} + \omega_p \frac{\partial^2 n_s}{\partial \omega_s^2}\right)}} \qquad 6.17$$

As seen from the equations above, longer samples will give a narrower gain bandwidth. The gain bandwidth will also become wider close to degeneracy. In the case of high gain, the bandwidth will be broaden with a factor $(1 + g^2L^2 / \pi^2)^{½}$ from the low gain value.

An OPO will in general have a narrower spectral bandwidth than an OPG, since the cavity itself acts like a filter and enhance the peak of the gain bandwidth more than the wings when the field is circulating in the cavity. Brosnan and Byer have given the following relation between the gain bandwidth $\Delta\omega_s$ and the total spectral bandwidth $\Delta\omega_{s,tot}$ for an OPO without additional optical elements in the cavity[73].

$$\Delta\omega_{s,tot} = \frac{1}{\sqrt{p_N}}\Delta\omega_s \qquad 6.18$$

p_N is the total number of roundtrips for the signal pulse in the cavity. The bandwidths above have all the inherent assumption that the pump beam is collimated. The bandwidth can increase considerably for divergent pump beams.

The spectral bandwidths of the constructed OPOs have been investigated in several of the presented papers. In paper [V] the specific goal was to construct a narrow bandwidth PPKTP OPO that operated on only one axial mode. The reason was that such coherent tuneable light sources have many applications in high-resolution spectroscopy and LIDAR applications. The spectral bandwidths from nanosecond OPOs are usually too broad to use directly, if no additional elements to filter the spectrum is included in the cavity. We pumped a 17 mm long PPKTP crystal with an injection seeded Nd:YAG laser, 12 ns, 10 Hz and $M^2 \approx 1.1$. The cavity was resonant for the signal and consisted of two flat mirrors and a reflection grating. This cavity configuration works as a spectral filter and allows only a very narrow part of the spectrum to pass with small losses back and forth in the cavity. An additional benefit of the configuration is that the OPO is possible to tune by tilting of the output mirror, the grating will after the slight rotation filter out a different part of the spectrum. This tuning is possible under the entire gain bandwidth of the material. The OPO in our paper was operating on a single longitudinal mode and was tuneable over 1300 GHz around 1.685 μm. The spectral bandwidth was measured to be $\Delta\nu_{s,tot} < 400$ MHz. This radiation was then amplified in a second PPKTP crystal of 20 mm length and the same pump laser was used. After the amplification the signal pulse energy increased almost 6 times to 2.15 mJ and the spectral bandwidth and tuning characteristics were left unchanged. The total conversion efficiency reached 30 %. The beam quality of the signal was $M^2 = 1.4$. Figure 6.8 shows the line profile of the SRO taken through the fringe pattern produced by a 5 GHz free spectral range Fabry-Perot interferometer.

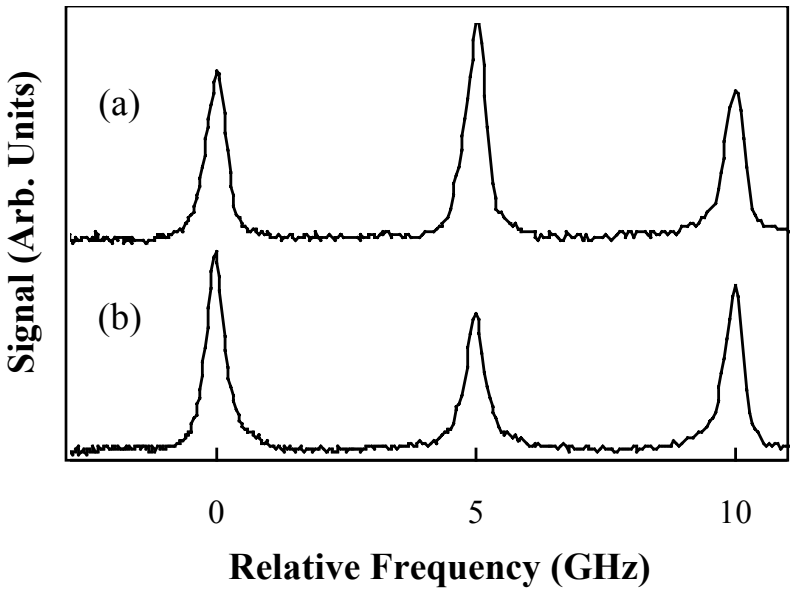

Fig. 6.8 Spectrum from Fabry-Perot interferometer. The free spectral range is 5 GHz. (a) OPO. (b) amplified OPO signal.

The spectra that are shown are actually from the sum frequency mixing of the signal and the pump, which for the interferometer gave a detectable wavelength around 0.652 μm. The line profiles are narrower than the resolution limit of the interferometer, which is 400 MHz. The true signal bandwidth is hence smaller than that value.

6.11 Parasitic processes

As mentioned earlier in paragraph 3.4 parasitic processes have been observed in the OPOs and OPAs in this thesis work. Second order nonlinear mixing processes of all kinds have been seen. Most of them have been non-phasematched. The generated wavelengths, although most of the time very weak, have made the output colourful. The front page of this thesis shows the output from the PPKTP OPO in paper [II]. The SRO was pumped at 1.064 μm and generated 1.72 and 2.8 μm, which of course is invisible to the human eye. The green light in the middle comes from non-phasematched frequency doubling of the pump beam. The red ring around the centre has a wavelength of 0.678 μm and the half-angle of the cone is 0.8°. Through calculations of the non-collinear phasematching geometry, we came to the conclusion that the origin of the red ring is from non-phasematched 2^{nd} order SFG of the pump wave and a signal wave at 1.869 μm that is propagating at 1.25° towards the x-axis (internal angle). The same OPO also exhibited even weaker blue and ultraviolet wavelengths as well as several lines in the infrared, when the generated beams were dispersed through a prism. However, the total power of the parasitic wavelengths was less than 1 mW compared to the signal and idler output that was ~250 mW. High-order processes originating from the second order susceptibility is something that has to be considered when the QPM grating is designed and they could be detrimental to the desired process if the circumstances are bad.

We have also observed a parasitic process originating from the third order susceptibility. In the OPO constructed in paper [III] with the high finesse cavity Stimulated Raman Scattering (SRS) was detected. We found an additional line shifted from the signal line at 1.544 μm. The shift corresponds well with the reported Stokes shift of 269 cm^{-1} in KTP for this polarisation configuration[112]. The power in the Stokes shifted line was approximately 50 % smaller than the signal power at four times the OPO threshold and it was extremely sensitive to the cavity alignment. This indicates that the SRS process was supported by the wide bandwidth of the cavity mirrors. We believe that if mirrors, which were anti-reflection coated at the shifted wavelength of 1.61 μm and highly reflective around 1.54 μm, had been used the SRS would have disappeared. This OPO in paper [III] is the only OPO pumped in the infrared where we have been able to detect SRS. An important feature of Raman generation is that Δk is identically zero, which means that the Raman generated wave easily can grow strong.

6.12 Femtosecond pulses

Although, the generation of ultrashort pulses has not been the main topic of this study, I will here discuss the subject very briefly, since a travelling-wave OPA in the femtosecond regime was reported in paper [VIII]. The spectral width that the optical pulses possess can not be neglected any longer when the pulses become sufficiently short. This happens when the pulse width is on the order of 1 - 10 picoseconds. The magnitude of the wavevector will then depend on frequency. In order to deduce the coupled wave equations for nonlinear mixing phenomena, the wavevectors have to be expanded in Taylor series around their centre frequencies[113]. In the infinite plane wave limit and after SVEA has been applied the coupled wave equations for the second order susceptibility in the adiabatic limit can be written analogous to equation 2.8 [3]:

$$
\begin{aligned}
i\left(\frac{\partial}{\partial x}+\frac{dk_1}{d\omega_1}\frac{\partial}{\partial t}\right)E_1(t)-\tfrac{1}{2}\frac{d^2k_1}{d\omega_1^2}\frac{\partial^2}{\partial t^2}E_1(t)+\ldots &= -\frac{\omega_1^2}{k_1c^2}Kd_{eff}E_3(t)E_2^*(t)\exp(i\Delta k_{tot}x)\\
i\left(\frac{\partial}{\partial x}+\frac{dk_2}{d\omega_2}\frac{\partial}{\partial t}\right)E_2(t)-\tfrac{1}{2}\frac{d^2k_2}{d\omega_2^2}\frac{\partial^2}{\partial t^2}E_2(t)+\ldots &= -\frac{\omega_2^2}{k_2c^2}Kd_{eff}E_3(t)E_1^*(t)\exp(i\Delta k_{tot}x) \qquad 6.19\\
i\left(\frac{\partial}{\partial x}+\frac{dk_3}{d\omega_3}\frac{\partial}{\partial t}\right)E_3(t)-\tfrac{1}{2}\frac{d^2k_3}{d\omega_3^2}\frac{\partial^2}{\partial t^2}E_3(t)+\ldots &= -\frac{\omega_3^2}{k_3c^2}Kd_{eff}E_1(t)E_2(t)\exp(-i\Delta k_{tot}x)
\end{aligned}
$$

The phase-mismatch equals $\Delta k_{tot} = k_3-k_2-k_1-K_m$ and the frequency relation is $\omega_3 = \omega_1+\omega_2$. The derivative $(dk/d\omega)^{-1} = v_g$ is the group velocity of the pulse envelope. The second derivative $d^2k/d\omega^2$ is the group velocity dispersion (GVD) and it is a measure of how fast the spectral components of the pulse will drift apart, i.e. this derivative is responsible for the linear pulse broadening when the pulse propagates through a medium.

It is necessary to have a high nonlinear coefficient, phasematching of the process and in addition for femtosecond interactions a small mismatch between the group velocities of the interacting fields to receive an efficient frequency conversion.

Furthermore, the GVD and higher-order terms must be sufficiently small so they can be neglected or they have to be compensated for during the experiments.

The properties of PPKTP make it a very strong candidate to use in an amplifier for femtosecond pulses. Foremost, it is the materials high nonlinear coefficient and its high optical damage threshold that are attractive features. In addition the group velocity mismatch (GVM) at the wavelengths of the amplifier in paper [VIII] were favourable. The GVM is defined as:

$$GVM = \left(\frac{1}{v_{g,p}} - \frac{1}{v_{g,s,i}} \right) \qquad 6.20$$

$v_{g,j}$ j = p, s or i stand for the group velocity of the pump, signal or idler, respectively. The GVM between the pump and signal was approximately 120 fs/mm and almost 0 fs/mm for the GVM between the pump and idler. Because of these parameters the PPKTP sample in the OPA could have a length of 4 mm. A longer sample would have suffered from the negative effects of GVM and GVD, since they increase with distance for a sample poled with a constant period. In the reported amplifier we generated 210 fs long pulses at 3.8 μm and the received idler pulse energy was 5 μJ. The sample was pumped by a Ti:Sapphire regenerative amplifier that produced ~100 fs long pulses tuneable around 0.8 μm and with maximum pulse energy of 75 μJ. These pulses were mixed with narrow-band 1 ns pulses at 1.064 μm and 8 μJ energy. The internal conversion efficiency was 40 % and the idler pulses had a time-bandwidth product that was only 20% from the value of the time-bandwidth product of the pump pulses. This OPA was the first high power femtosecond PPKTP OPA generating in the mid-infrared spectral region. The output characteristics of the device reported here have only been matched by a MgO:PPLN OPO, which produced ~10 μJ at wavelengths around 3.5 μm, that sample was 10 mm long[114].

7 Description of the original research work

Paper I: Efficient nanosecond optical parametric oscillators based on periodically poled KTP, emitting in the 1.8 – 2.5 μm spectral region.

J. Hellström, V. Pasiskevicius, F. Laurell, and H. Karlsson, Opt. Lett., **24**, 1233-1235 (1999).

Optical parametric oscillators in periodically poled $KTiOPO_4$ pumped by a nanosecond Q-switched Nd:YAG laser were demonstrated for the first time. Two crystals (A and B) with the same period 38.5 μm were fabricated and their effective non-linear coefficients were deduced from experiments to be 6.3 pm/V and 8.7 pm/V, respectively. The maximum output pulse energy from the OPO in the forward direction was 1.2 mJ, corresponding to 34 % conversion efficiency from 1.064 μm. The signal (idler) was tunable from 1.85 μm (2.51 μm) to 1.92 μm (2.39 μm) by changing the temperature from 10 to 100 °C. An investigation of the temporal depletion of the pump pulses was also performed.

Paper II: High-power optical parametric oscillation in large-aperture periodically poled $KTiOPO_4$

J. Hellström, V. Pasiskevicius, H. Karlsson, and F. Laurell, Opt. Lett., **25**, 174-176 (2000).

The first electric field poling of a large aperture (3 mm thick, 2 mm wide) $KTiOPO_4$ crystal was reported and the output energies of the constructed OPO was scaled approximately one order of magnitude from the milijoule range in paper [I]. The maximum beam radius at the waist was 1.1 mm and this made it possible to use all of the pump energy (28.5 mJ) from the flash-lamp pumped Nd:YAG pump laser. Maximum output pulse energy in the forward direction was 12.5 mJ (signal + idler). The total conversion efficiency reached 45 %. We evaluated the homogeneity of the poled volume by high-order second harmonic generation experiments and found the uniformity to be excellent. An investigation of the output beam quality in relation to cavity lengths and beam waist radii was also made.

Paper III: Optical parametric amplification in periodically poled $KTiOPO_4$, seeded by an Er-Yb:glass microchip laser

J. Hellström, G. Karlsson, V. Pasiskevicius, and F. Laurell, Opt. Lett., **26**, 352-354 (2001).

A detailed investigation of an optical parametric amplifier in periodically poled $KTiOPO_4$ is presented. An OPA has the potential of providing better and simpler control of the output spectrum than a parametric oscillator The crystal was pumped by a Q-switched Nd:YAG laser with 5 ns pulses and seeded by 6 mW (1.544 μm) from an Er-Yb:glass microchip laser. The OPA provided 66 dB amplification and produced

pulses of 3 ns and peak powers of up to 24 kW. The effective non-linear coefficient was found from experiments to be 9.7 pm/V, this is the highest value reported for a PPKTP parametric device so far. A drawback of the device was that a significant amount of parasitic second harmonic generation from the pump was produced, especially at elevated temperatures. In addition, Stimulated Raman Scattering was observed as a parasitic process in an OPO that was constructed with the same crystal.

Paper IV: Real-time and *in situ* monitoring of ferroelectric domains during periodic electric field poling of $KTiOPO_4$

J. Hellström, R. Clemens, V. Pasiskevicius, H. Karlsson, and F. Laurell, J. Appl. Phys., **90**, 1489-1495 (2001).

A new photographic method for monitoring the reversal of ferroelectric domains during electric field poling of $KTiOPO_4$ was developed. The technique provided the possibility to view the formation of inverted domains *in situ* and in real time. A beam from a He-Ne laser was directed through the crystal perpendicular to both the QPM grating vector and the patterned surface. The electro-optic effect was utilized to receive a difference in intensity between adjacent half-periods during poling and an image of the grating was formed on a matrix charge coupled device (128 by 128 pixels). After poling the sample could be probed by applying a voltage that was lower than the coercive field of the crystal. This probing revealed the quality of the poled grating. Furthermore we found, both in non-poled and poled samples, that space charges were injected periodically into the samples when the voltage was applied. The charges created a weak periodic pattern, which decayed with time. Approximate values of the relaxation constant for the decay of the space charge fields were determined to be on the milisecond level, in agreement with predictions from theory. The fast relaxation requires the use of short poling pulses to prevent domain broadening.

Paper V: Single mode near infrared optical parametric oscillator–amplifier based on periodically poled $KTiOPO_4$

G. W. Baxter, P. Schlup, I. T. McKinnie, J. Hellström, and F. Laurell, Accepted for publication in Appl. Opt., Dec, (2001).

In these experiments we constructed an optical parametric oscillator operating on a single axial mode. The OPO was passively line narrowed by a diffraction grating in grazing incidence configuration and pumped by a Q-switched, injection seeded Nd:YAG laser at 10 Hz repetition rate. A 17 mm long periodically poled $KTiOPO_4$ crystal served as the gain medium, Λ = 37.4 μm. A Fabry-Perot interferometer confirmed that the near-infrared OPO was single mode at 1.68 μm and that the bandwidth was less than 400 MHz. The OPO was tuned by tilting the output mirror and it remained single mode over a 12 nm tuning range, almost its entire bandwidth. The signal output energy reached up to 0.37 mJ when pumped by 3.1 mJ and the slope efficiency was 46 %. M^2 = 1.6 for the signal. The output radiation was amplified in a second PPKTP crystal (20 mm long). The amplified signal (idler) output was 2.15 mJ

(1.18 mJ) for 11 mJ pump pulses. The bandwidth and beam quality was completely preserved for this second stage.

Paper VI: Widely and continuously tuneable optical parametric oscillator using a cylindrical periodically poled $KTiOPO_4$ crystal

J.-P. Fève, O. Pacaud, B. Boulanger, B. Ménaert, J. Hellström, V. Pasiskevicius, and F. Laurell, Accepted for publication in Opt. Lett., Dec. (2001).

In this paper we published the first realisation of a periodically poled crystal with a cylindrical shape in an OPO. The poled region of the sample had an area of 10 by 10 mm^2 and the thickness was 0.5 mm. The geometry of the PPKTP crystal made it possible to continuously tune the signal (idler) wavelength 523 nm (1340 nm) by rotating the sample 26° from the cavity axis. This is the widest tuning so far in a PPKTP OPO and it is comparable to the widest tuning reported for PPLN OPOs. The OPO was pumped by a Nd:YAG laser at 1.064 μm with 6 ns pulses at a repetition rate of 10 Hz. The quality of the pump beam was $M^2 \approx 1.1$. The OPO converted at maximum 17.3 % of the pump energy to output pulse energy when pumped with 0.43 mJ at a rotation angle of 26°. The threshold intensity of the OPO was essentially constant throughout the tuning range, which also indicated a homogeneous poling of the crystal. The advantages with this cavity and crystal design are that truly continuous tuning of the output wavelengths is achieved over a wide spectral range without any substantial lateral walk-off between the interacting waves.

Paper VII: Optical parametric oscillators for high pulse energy and high average power operation based on large aperture periodically poled KTP and RTA

M. Peltz, U. Bäder, A. Borsutzky, R. Wallenstein, J. Hellström, H. Karlsson, V. Pasiskevicius, and F. Laurell, Accepted for publication in Appl. Phys. B.

A thorough investigation of the performance of two large aperture periodically poled crystals in optical parametric oscillators was presented. The poled volumes were 8 x 2 x 3 mm^3 for the PPKTP sample and 7 x 3 x 3 mm^3 for the PPRTA. Two-dimensional spatial mapping of the total OPO output power, the signal wavelength and signal bandwidth as a function of the crystal position indicated a good uniformity of the quasi-phasematched structure in the entire poled volume. We used a high repetition rate, diode-pumped Nd:YVO_4 laser to pump the OPO cavities with 7.2 and 8 W respectively. This gave a maximum output average power of 2 and 1.3 W. Because of the homogeneity of the poled gratings we could scale up the output pulse energies by pumping with low repetition rate lasers with large beam diameters. This resulted in up to 18 mJ in output pulse energy and total conversion efficiencies of 38 %. New coefficients for the temperature dispersion equations for RTA were also presented.

Paper VIII: Efficient femtosecond travelling-wave optical parametric amplification in periodically poled $KTiOPO_4$

F. Rotermund, V. Petrov, F. Noack, V. Pasiskevicius, J. Hellström, and F. Laurell, Opt. Lett. **24**, 1874-1876 (1999).

This paper was the first report on a high-power, femtosecond, travelling wave optical parametric amplifier that used a periodically poled $KTiOPO_4$ crystal as nonlinear material. The sample length was 4mm. Approx. 100 fs long pulses from a Ti:sapphire regenerative amplifier at around 0.8 μm were mixed together with 1 ns pulses from a Q-switched microlaser at 1.064 μm. An idler at 3.8 μm was generated in the amplification process and 5 μJ pulses were achieved from 75 μJ input. This corresponded to 40 % total internal conversion efficiency. The idler pulses were approx. 210 fs long and had a time-bandwidth product of 0.6 (0.5 for the pump pulses). Up to 10 % of the pump energy was found to be frequency doubled in a parasitic 9:th-order SHG process. Another process, which could be detrimental to the amplification process, was the observed formation of grey-tracks at high intensities and at room temperature, however no permanent damage occurred. No grey-tracks could be found at elevated temperatures, (120 °C). The output characteristics of the device reported here have only been matched by a MgO:PPLN OPO, which produced ~10 μJ at wavelengths around 3.5 μm, that sample was 10 mm long.

Paper IX: Noncollinear optical parametric oscillator with periodically poled KTP

V. Smilgevičius, A.Stabinis, A. Piskarskas, V. Pasiskevicius, J. Hellström, S. Wang, and F.Laurell, Opt. Comm. **173**, 365-369 (2000).

Here we characterized a quasi-phasematched optical parametric oscillator in a noncollinear configuration. An advantage with noncollinear phasematching is that tuning can be achieved without changing the temperature of the sample. The pump beam from a nanosecond frequency doubled Nd:YAG laser was kept collinear with the grating vector of the PPKTP crystal, while the cavity axis could have an angle θ towards this first axis. The OPO was operating in degenerate mode at $\theta = 0°$ and room temperature and converted 50 % of the pump pulse energy ($E_p \approx 300$ μJ) to the near infrared. The total tuning range at room temperature was 184 nm when the crystal was rotated 5.6°. At an angle $\theta = 1.2°$ the noncollinear OPO still had a total efficiency of 40 %. An investigation of the threshold behavior versus cavity angle and different pump beam radii was also carried out. Equations for finding the correct cavity angle θ for given temperature and wavelength was also presented.

8 Contributions by the candidate

Paper I:

The candidate and V. Pasiskevicius made the design of the OPOs and performed the experiments together. The candidate poled the crystal called “A”, while H. Karlsson poled sample “B”. The candidate also made the simulations of the OPO thresholds and was responsible for writing the paper.

Paper II:

The candidate performed the experiments and simulations together with V. Pasiskevicius. H. Karlsson poled the crystal. The candidate and V. Pasiskevicus wrote the paper.

Paper III:

I designed the OPO and the OPA, fabricated and evaluated the crystal and was responsible for all the experiments. G. Karlsson constructed and characterised the Er-Yb:glass microchip laser and V. Pasiskevicius helped out with the measurements of the optical bandwidths. I was responsible for writing the paper.

Paper IV:

I designed the experimental set-up, prepared and poled the samples. I also made the theoretical calculations, evaluated the poled crystals in OPOs and wrote the paper. R. Clemens participated in some experiments and in the discussion of the results. V. Pasiskevicius contributed to the theory and the discussion and H. Karlsson came with the original idea to take pictures of the domains.

Paper V:

The candidate poled the crystal and made an initial evaluation of the sample for the OPO. G. W. Baxter and P. Schlup made the OPO and OPA experiments. The candidate and P. Schlup wrote the paper.

Paper VI:

I performed the poling of the large area crystal and made an evaluation of the sample in an OPO. The French group polished the crystal and made the OPO experiments. J.-P. Fève and I wrote and discussed the theory thoroughly, with advice from V. Pasiskevicius.

Paper VII:

The candidate and M. Peltz designed and performed all the experiments with the PPKTP crystal. H. Karlsson poled both crystals and made the PPRTA experiments together with U. Bäder. The candidate and M. Peltz wrote the paper.

Paper VIII:

I prepared the crystal and participated in the discussion of the paper. V. Pasiskevicius performed the OPA experiments and wrote the paper together with the group from Germany.

Paper IX:

The candidate participated in the experiments as well as in the discussion of the paper. V. Pasiscevicius was the principal investigator and he also wrote the paper. The group from Lithuania contributed mainly in the theoretical part of the article. S. Wang prepared the crystal.

9 Conclusions

The main conclusion of this thesis is that periodically poled KTP is a suitable material to use in nanosecond optical parametric oscillators and amplifiers.

The material properties that make KTP an attractive nonlinear crystal to use in QPM OPOs and OPAs are foremost: The relatively large value of the nonlinear coefficient d_{33}, the high resistance to optically induced breakdown, the low susceptibility to grey-track formation, insensitivity to the photorefractive effect, its wide transparency and perhaps most importantly, its low coercive field. These properties make it possible to pole thick crystals and operate the parametric devices at room-temperature.

It has been shown in this thesis that it is possible to pole large volumes of KTP with a high quality of the quasi-phasematched grating. The highest value of the effective nonlinear coefficient measured in this work is 9.7 pm/V, which is the largest value reported for a PPKTP parametric device so far and is only 10 % less than the maximum possible value calculated from the d_{33} of non-poled KTP. Highly efficient nanosecond OPOs have been constructed around a 3 mm thick PPKTP sample, where maximum conversion efficiencies have reached 45 % in the case of a singly resonant OPO. Total pulse energies for both the signal and the idler of up to 18 mJ have been demonstrated at 35 % conversion efficiency. A possible application for such pulses could be in long distance LIDAR measurements for environmental monitoring. An average output power of 2 W has been published for a SRO generating at 1.72 μm and 2.8 μm. However, up to 24 W has been produced in experiments which have yet to be published, in a doubly resonant OPO operating close to degeneracy. The efficiency reached 48 % in this case. For the first time has a periodically poled crystal been polished into a cylindrical shape and used as nonlinear material in an OPO. This type of OPO provides truly continuous and very wide spectral tuning. The total tuning range was 1.8 μm in the mid-infrared region, which is comparable with the record reported for PPLN OPOs pumped at the same wavelength. It was also shown that PPKTP provides enough parametric gain to build an OPO with a very narrow bandwidth. Hence, this thesis shows that it should be possible to construct a nanosecond PPKTP OPO in a 3 mm thick crystal, which can exhibit a large tuning range, narrow bandwidth and produce both high average power and high pulse energies in the same device.

Furthermore, it has been shown that PPKTP has suitable values of GVM and GVD for efficient generation of femtosecond pulses in the mid-infrared spectral region. 5 μJ pulses at 3.8 μm were generated with 40 % internal efficiency in a 4 mm long PPKTP OPA.

Parasitic processes were observed in some of the constructed devices during the course of this project, although they had little affect on the operation of the device. Nevertheless they should be considered when designing the periodically poled crystal and the cavity. The parasitic processes have been high-order frequency mixing processes and in one case Raman generation.

A photographic method to view the inversion of the ferroelectric domains during the periodic electric field poling of KTP has been reported as well. The method takes

advantage of the electro-optic effect and a high-speed CCD camera. The technique allows monitoring *in-situ* and in real time and each half-period of the QPM grating can be observed. The method provides the opportunity to monitor the dynamics of the domains during poling and conduct a non-invasive evaluation of the grating afterwards. This method should be applicable to other ferroelectric crystals too. The experiments indicate that the dielectric relaxation time in KTP is on the order of 1 to 10 ms, which is in agreement with what was anticipated from calculations.

It should be pointed out that when comparing PPKTP to other nonlinear materials PPKTP has many benefits, but also some disadvantages. PPLN is still the most extensively used periodically poled material and is still ahead of PPKTP in many ways. PPLN is already a commercial product, but several companies are working at taking PPKTP from the research laboratory to the market. The largest obstacles are that entire KTP wafers cannot yet be poled at room-temperature and that the material properties varies somewhat over the wafer area. Future research efforts have to address these problems.

References

[1] A. L. Schawlow and C. H. Townes, *Phys. Rev*., **112**, 1940 (1958).

[2] T. H. Maiman, *Nature*, **187**, 493 (1960).

[3] P. N. Butcher and D. Cotter, "*The Elements of Nonlinear Optics*", Eds: P. L. Knight and W. J. Firth, Cambridge Studies in Modern Optics 9, Cambridge University Press, UK (1990).

[4] A. Yariv, "*Quantum electronics*", 3:rd ed, John Wiley & sons, Singapore (1988).

[5] R. L. Byer, "*Quantum electronics: a treatise*", Eds: H. Rabin and C. L. Tang, nonlinear optics, vol. 1, part B, Academic Press, New York, pp. 588-703 (1975).

[6] R. L. Byer, "*Nonlinear optics*" Eds: P. G. Harper and B. S. Wherrett, Academic Press, New York, pp. 47-161, (1977).

[7] D. A. Kleinman, *Phys. Rev*., **126** 1977 (1962).

[8] Y. R. Shen, "*The principles of Nonlinear Optics*", John Wiley & sons, USA (1984).

[9] G. D. Boyd and D. A. Kleinman, *J. Appl. Phys.*, **39**, 3597 (1968).

[10] J. A. Armstrong, N. Bloembergen, J. Ducuing, and P. S. Pershan, *Phys. Rev.*, **127**, 1918 (1962).

[11] D. K. Cheng, "*Field and Wave Electromagnetics*", 2:nd, Addison-Wesley, USA, (1989).

[12] M. V. Hobden, *J. Appl. Phys*, **38**, 4365 (1967).

[13] R. L. Sutherland, "*Handbook of Nonlinear Optics*", Ed: B. J. Thompson, Optical Engineering, Marcel Dekker, USA, (1996).

[14] P. A. Franken and J. F. Ward, *Rev. Mod. Phys*., **35,** 23 (1963).

[15] M. M. Fejer, G. A. Magel, D. H. Jundt, and R. L. Byer, *IEEE J. Quantum Electron.*, **28**, 2631 (1992).

[16] L. A. Gordon, G. L. Woods, R. C. Eckardt, R. K. Route, R. S. Feigelson, M. M. Fejer, and R. L. Byer, *Electron Lett.* **29**, 1942 (1993).

[17] D. Zheng, L. A. Gordon, Y. S. Wu, R. S. Feigelson, M. M. Fejer, and R. L. Byer, *Opt. Lett.*, **23**, 1010 (1998).

[18] L. Becouarn, E. Lallier, M. Brevignon, and J. Lehoux, *Opt. Lett.*, **23**, 1508 (1998).

[19] B. F. Levine, C. G. Bethea, and R. A. Logan, *Appl. Phys. Lett.*, **26**, 375 (1975).

[20] Y-L. Lu, Y-Q. Lu, J-J. Zheng, C-C. Xue, X-F. Cheng, and G-P. Luo, *Appl. Phys. Lett.*, **69**, 1660 (1996).

[21] J. Webjörn, F. Laurell, and G. Arvidsson, *J. Lightwave Technol*., **7**, 1597 (1989).

[22] J. D. Bierlein, D. B. Laubacher, J. B. Brown, and C. J. van der Poel, *Appl. Phys. Lett.*, **56**, 1725 (1990).

[23] C. J. van der Poel, J. D. Bierlein, J. B. Brown, and S. Colak, *Appl. Phys. Lett.*, **57**, 2074 (1990).

[24] M. C. Gupta, W. P. Risk, A. C. G. Nutt, and S. D. Lau, *Appl. Phys. Lett.*, **63**, 1167 (1993).

[25] W.-Y. Hsu, and M. C. Gupta, *Appl. Phys. Lett.,* **60**, 1 (1992).

[26] A. C. G. Nutt, V. Gopalan, and M. C. Gupta, *Appl. Phys. Lett.,* **60**, 2828 (1992).

[27] M. Yamada, N. Nada, M. Saitoh, and K. Watanabe, *Appl. Phys. Lett.,* **62**, 435 (1993).
[28] J. Webjörn, V. Pruneri, P. S. J. Russel, J. R. M. Barr, and D. C. Hanna, *Electron. Lett*., **30**, 894 (1994).
[29] G. D. Miller, R. G. Batchko, M. M. Fejer, and R.L. Byer, SPIE **2700,** 34, (1996).
[30] L. E. Myers, R. C. Eckardt, M. M. Fejer, R. L. Byer, W. R. Bosenberg, and J. W. Pierce, *J. Opt. Soc. Am. B*, **12**, 2102 (1994).
[31] H. Karlsson and F. Laurell, *Appl. Phys. Lett.*, **71**, 3474 (1997).
[32] Q. Chen and W. P. Risk, *Electron. Lett*., **30**, 1516 (1994).
[33] G. Rosenman, A. Skliar, D. Eger, M. Oron, and M. Katz, *Appl. Phys. Lett.*, **73**, 3650 (1998).
[34] J.-P. Meyn, M. E. Klein, D. Woll, R. Wallenstein, and D. Rytz, *Opt. Lett.*, **24**, 1154 (1999).
[35] M. E. Klein, D.-H. Lee, J.-P. Meyn, B. Beier, K.-J. Boller, and R. Wallenstein, *Opt. Lett.*, **23**, 831 (1998).
[36] S. Wang, V. Pasiskevicius, F. Laurell, and H. Karlsson, *Opt. Lett.*, **23**, 1883 (1998).
[37] L. E. Myers, R. C. Eckardt, M. M. Fejer, Robert L. Byer, and W. R. Bosenberg, *Opt. Lett.*, **21**, 591 (1996).
[38] P. E. Powers, T. J. Kulp, and S. E. Bisson, *Opt. Lett.*, **23**, 159 (1998).
[39] M. Katz, A. Englander, and D. Eger, Conference Digest CLEO-Europe-2000, CThM3, 351 (2000).
[40] G. Imeshev, M. Proctor, and M. M. Fejer, *Opt. Lett.*, **23**, 673 (1998).
[41] M. A. Arbore, O. Marco, and M. M. Fejer, *Opt. Lett.*, **22**, 865 (1997).
[42] G. Imeshev, M. M. Fejer, A. Galvanauskas, and D. Harter *J. Opt. Soc. Am. B*, **18**, 534 (2001).
[43] G. W. Ross, N. G. Broderick, H. L. Offerhaus, P.G. R. Smith, D. J. Richardson, and D. C. Hanna, Technical Digest CLEO-00, CWH3, San Fransisco, USA, 274 (2000).
[44] S. Helmfrid, G. Arvidsson, and J. Webjörn, *J. Opt. Soc. Am. B*, **10**, 222 (1993).
[45] H. Karlsson, F. Laurell, P. Henriksson, and G. Arvidsson, *Electron. Lett.*, **32**, 556 (1996).
[46] K. Mizuuchi, K. Yamamoto, M. Kato, and H. Sato, *IEEE J. Quantum Electron.* **30**, 1596 (1994).
[47] L. Ouvrard and M. Troost, *Compt. Rend.*, **111**, 177 (1890).
[48] I. Tordjman, R. Masse, and J. C. Guitel, *Zeitschrift für Kristallographie*, **139**, 103 (1974).
[49] F. C. Zumsteg, J. D. Bierlein, and T. E. Gier, *J. Appl. Phys.*, **47**, 4980 (1976).
[50] J. D. Bierlein and C. B. Arweiler, *Appl. Phys. Lett.*, **49**, 917 (1986).
[51] D. A. Roberts, *IEEE J. Quantum Electron.*, **28**, 2057 (1992).
[52] J. D. Bierlein and H. Vanherzeele, *J. Opt. Soc. Am. B*, **6**, 622 (1989).
[53] M. Kunz, R. Dinnebier, L. K. Cheng, E. M. McCarron, D. E. Cox, J. B. Parise, M. Gehrke, J. Calabrese, P. W. Stephens, T. Vogt, and R. Papoular, *J. Solid State Chemistry*, **120**, 299 (1995).
[54] D. Xue and S. Zhang, *Appl. Phys. Lett.*, **70**, 943 (1997).

[55] J. Nordborg, "*Non-linear Optical Titanyl Arsenates, crystal growth and properties*", ISBN 91-7197-882-8, PhD-thesis, Chalmers University of Technology (2000).
[56] L. K. Cheng, L. T. Cheng, J. Galperin, P. A. Morris Hotsenpiller, and J. D. Bierlein, *J. Crystal Growth*, **137**, 107 (1994).
[57] M. N. Satyanarayan, A. Deepthy, and H. L. Bhat, *Critical Reviews in Solid State and Material Sciences*, **24**, 103 (1999).
[58] G. Rosenman, A. Skliar, and A. Arie, "*Ferroelectric Domain Engineering for Quasi-Phase-Matched Nonlinear Optical Devices*", Gordon and Breach Science Publications imprint, Malaysia, (1999).
[59] C. Kittel, "*Introduction to Solid State Physics*", 7:th ed, John Wiley and sons, USA, (1996).
[60] J. D. Bierlein and F. Ahmed, *Appl. Phys. Lett.*, **51**, 1322 (1987).
[61] V. K. Wadhawan, "*Introduction to ferroic materials*", Gordon and Breach Science publishers imprint, ISBN 90-5699-286-4, Singapore, (2000).
[62] P. Urenski, M. Lesnykh, Y. Rosenwaks, G. Rosenman, and M. Molotskii, *J. Appl. Phys.*, **90**, 1950 (2001).
[63] D. K. T. Chu, J. D. Bierlein, and R. G. Hunsperger, *IEEE Trans. Ultrasonics Ferroelectrics, Frequency Control,* **39**, 683 (1992).
[64] K. Fradkin, A. Arie, A. Skliar, and G. Rosenman, *Appl. Phys. Lett.*, **74**, 914 (1999).
[65] K. Fradkin-Kashi, A. Arie, P. Urenski, and G. Rosenman, *Opt. Lett.*, **25**, 743 (2000).
[66] K. Fradkin-Kashi, A. Arie, P. Urenski, and G. Rosenman, *Appl. Phys. B.*, **71**, 251 (2000).
[67] T. Y. Fan, C. E. Huang, B. Q. Hu, R. C. Eckardt, Y. X. Fan, R. L. Byer, and R. S. Feigelson, *Appl. Opt.*, **26**, 2390 (1987).
[68] V. G. Dimitrev, G. G. Gurzadyan, and D. N. Nikogosyan, "*Handbook of Nonlinear Optical Crystals*", Ed: A. E. Siegman, Springer series in optical sciences, Vol. 64, Springer-Verlag, Berlin Heidelberg, 1991.
[69] G. Ghosh, *IEEE Phot. Techn. Lett.*, **7**, 68 (1995).
[70] W. Wiechmann, S. Kubota, T. Fukui, and H. Masuda, *Opt. Lett.*, **18**, 1208 (1993).
[71] G. Hansson, H. Karlsson, S. Wang, and F. Laurell, *Appl. Opt.*, **39**, 5058 (2000).
[72] H. Karlsson, "*Fabrication of periodically polde crystals from the KTP family and their applications in nonlinear optics*", PhD-thesis, TRITA-FYS 2197, The Royal Institute of Technology, (1999).
[73] S. J. Brosnan and R. L. Byer, *IEEE J. Quantum Electron.*, **15**, 415 (1979).
[74] A. M. Glass, *Opt. Eng.*, **17**, 470 (1978).
[75] L. E. Myers and W. R. Bosenberg, *IEEE J. Quantum Electron.*, **33**, 1663 (1997).
[76] M. Taya, M. C. Bashaw, and M. M. Fejer, *Opt. Lett.*, **21**, 857 (1996).
[77] M. G. Roelofs, *J. Appl. Phys.*, **65**, 4976 (1989).
[78] B. Boulanger, M. M. Fejer, R. Blachman, and P. F. Bordui, *Appl. Phys. Lett.*, **65**, 2401 (1994).
[79] B. Boulanger, I. Rousseau, J. P. Fève, M. Maglione, B. Ménaert, and G. Marnier, *IEEE J. Quantum Electron.*, **35**, 281 (1999).

[80] V. Pasiskevicius, H. Karlsson, F. Laurell, R. Butkus, V. Smilgevicius, A. Piskarskas, *Opt. Lett.*, **26**, 710 (2001).
[81] G. Rosenman, Kh. Garb, A. Skliar, M. Oron, D. Eger, and M. Katz, *Appl Phys. Lett.*, **73**, 865 (1998).
[82] M. J. Missey, S. Russell, V. Dominic, R. G. Batchko, *Opt. Express*., **6**, 186 (2000).
[83] R. Stolzenberger and M. Scripsick, SPIE **3610**, 23 (1999).
[84] H. Karlsson, F. Laurell, and L. K. Cheng, *Appl. Phys. Lett.*, **74**, 1519 (1999).
[85] P. A. Franken, A. E. Hill, C. W. Peters, and G. Weinreich, *Phys. Rev. Lett.*, **7**, 118 (1961).
[86] J. A. Giordmaine and R. C. Miller, *Phys. Rev. Lett.*, **14**, 973 (1965).
[87] S. E. Harris, *Proc. IEEE*, December 2096 (1969).
[88] L. E. Myers, G. D. Miller, R. C. Eckardt, M. M. Fejer, R. L. Byer, and W. R. Bosenberg, *Opt. Lett.*, **20**, 52 (1995).
[89] T. Kartaloglu, K. G. Köprülü, O. Aytür, M. Sundheimer, W. P. Risk, *Opt. Lett.*, **23**, 61 (1998).
[90] A. Garashi, A. Arie, A. Skliar, and G. Rosenman, *Opt. Lett.*, **23**, 1739 (1998).
[91] D. T. Reid, Z. Penman, M. Ebrahimzadeh, W. Sibbett, H. Karlsson, and F. Laurell, *Opt. Lett.*, **22**, 1397 (1997).
[92] G. Rosenman, A. Skliar, Y. Findling, P. Urenski, A. Englander, P. A. Thomas, and Z. W. Hu, *J. Phys. D: Appl. Phys.*, **32**, L49-L52 (1999).
[93] M. J. Missey, V. Dominic, L. E. Myers, and R. C. Eckardt, *Opt. Lett.*, **23**, 664 (1998).
[94] Y. Hirano, S. Yamamoto, T. Taijime, H. Taniguchi, M. Nakamura, *Postdeadline papers,* CLEO-00, CPD7, San Fransisco, USA, 13 (2000).
[95] Y. Furukawa, M. Nakamura, S. Takekawa, K. Kitamura, H. Hatanaka, K. Nakamura, H. Ito, A. Alexandrovski and M. M. Fejer, *Trends in Optics and Photonics*, **50**, 685, 2001.
[96] M. Peltz, J.-P. Meyn, U. Bäder, T. Bauer, A. Borsutzky, R. Wallenstein, D. Rytz, *Technical Digest*, CLEO-00, CMC3, San Fransisco, USA, 11 (2000).
[97] A. Fix, T. Schröder, and R. Wallenstein, *Laser Optoelektron.*, **23**, 106 (1991).
[98] Y. Suzaki and A. Tachibana, *Appl. Opt.*, **14**, 2809 (1975).
[99] T. F. Johnston, Jr, *Appl. Opt.*, **37**, 4840 (1998).
[100] G. Karlsson, V. Pasiskevicius, F. Laurell, J. A. Tellefsen, B. I. Denker, B. Galagan, V. V. Osiko, and S. Sverchkov, *Appl. Opt.*, **39**, 6188 (2000).
[101] A. V. Smith, Proc. SPIE **3928**, 62 (2000).
[102] A. E. Siegman, "*Lasers*", University Science Books, Sausalito, California, USA, (1986).
[103] G. Breitenbach, S. Schiller, and J. Mlynek, *J. Opt. Soc. Am. B*, **12**, 2095 (1995).
[104] L. R. Marshall, J. Kasinski, A. D. Hays, and R. Burnham, *Opt. Lett.* **16**, 681 (1991).

[105] P. B. Phua, B. X. Xu, T. C. Chong, and Y. C. Fong, *Opt. Comm.*, **139**, 320 (1997).
[106] L. E. Myers, R. C. Eckardt, M. M. Fejer, R. L. Byer, and W. R. Bosenberg, *Opt. Lett.*, **21**, 591 (1996).
[107] J. E. Bjorkholm, *IEEE J. Quantum Electron.*, **QE-7**, 109 (1971).
[108] J. A. C. Terry, Y. Cui, Y. Yang, W. Sibbett, and M. H. Dunn, *J. Opt. Soc. Am. B*, **11**, 758 (1994).
[109] A. V. Smith, W. J. Alford, T. D. Raymond, and M. S. Bowers, *J. Opt. Soc. Am. B*, **12**, 2253 (1995).
[110] W. Koechner, "*Solid-state Laser Engineering 4:ed*", Springer Series in Optical Sciences, Ed: H. K. V. Lotsch, **1**, 651, Springer-Verlag, Heidelberg, Germany (1996).
[111] Y. Hirano, S. Yamamoto, and H. Taniguchi, *Technical Digest*, CLEO-01, CFH2, Baltimore, Maryland, USA, 579 (2001).
[112] G. A. Massey, T. M. Loehr, L. J. Willis, and J. C. Johnson, *Appl. Opt.*, **19**, 4136 (1980).
[113] C. Hirlimann, "*Femtosecond Laser Pulses, principles and experiments"*, Ed: C. Rullière, p 26, Springer-Verlag, Berlin – Heidelberg, 1998.
[114] F. Rotermund, V. Petrov, F. Noack, M. Wittmann, and G. Korn, *Opt. Lett.*, **16**, 1539 (1999).